January 2015

An Improved Method For Estimating Aerosol Optical Thickness From Artificial Light Sources Observed By The Visible/infrared Imaging Radiometer Suite

Theodore Mitchell Mchardy

AN IMPROVED METHOD FOR ESTIMATING AEROSOL OPTICAL THICKNESS FROM ARTIFICIAL LIGHT SOURCES OBSERVED BY THE VISIBLE/INFRARED IMAGING RADIOMETER SUITE DAY/NIGHT BAND

by

Theodore Mitchell McHardy
Bachelor of Science, Cornell University, 2013

A Thesis

Submitted to the Graduate Faculty

of the

University of North Dakota

in partial fulfillment of the requirements

for the degree of

Master of Science

Grand Forks, North Dakota
December
2015

This thesis, submitted by Theodore Mitchell McHardy in partial fulfillment of the requirements for the Degree of Master of Science from the University of North Dakota, has been read by the Faculty Advisory Committee under whom the work has been done and is hereby approved.

Dr. Jianglong Zhang

Dr. Edward Hyer

Dr. Aaron Kennedy

This thesis is being submitted by the appointed advisory committee as having met all of the requirements of the School of Graduate Studies at the University of North Dakota and is hereby approved.

Wayne Swisher
Dean of the School of Graduate Studies

Date

PERMISSION

Title	An Improved Method for Estimating Aerosol Optical Thickness from Artificial Light Sources Observed by the Visible/Infrared Imaging Radiometer Suite Day/Night Band
Department	Atmospheric Sciences
Degree	Master of Science

In presenting this thesis in partial fulfillment of the requirements for a graduate degree from the University of North Dakota, I agree that the library of this University shall make it freely available for inspection. I further agree that permission for extensive copying for scholarly purposes may be granted by the professor who supervised my thesis work or, in her absence, by the Chairperson of the department or the dean of the School of Graduate Studies. It is understood that any copying or publication or other use of this thesis or part thereof for financial gain shall not be allowed without my written permission. It is also understood that due recognition shall be given to me and to the University of North Dakota in any scholarly use which may be made of any material in my thesis.

Theodore Mitchell McHardy
December 10, 2015

Table of Contents

List of Figures

List of Tables

ACKNOWLEDGMENTS

I would like to thank my advisor, Dr. Jianglong Zhang, for guiding me through my graduate work, as well as my other committee members, Drs. Edward Hyer and Aaron Kennedy. I also thank my friends and family for their support and ability to put up with me.

ABSTRACT

Using Visible/Infrared Imaging Radiometer Suite (VIIRS) Day/Night Band (DNB) data, a method, dubbed the "variance method", is developed for retrieving nighttime aerosol optical thickness (AOT) values based on the dispersion of radiance values above an artificial light source. An improvement of a previous algorithm, this updated method derives a semi-quantitative indicator of nighttime AOT using artificial light sources. Nighttime AOT retrievals from the newly developed method are inter-compared with an interpolated value from late afternoon and early morning ground observations from four AErosol RObotic NETwork (AERONET) sites as well as column-integrated Aerosol Optical Depth (AOD) from one High Spectral Resolution LiDAR (HSRL) site at Huntsville, AL during the NASA Studies of Emissions and Atmospheric Composition, Clouds and Climate Coupling by Regional Surveys (SEAC^{4}RS) campaign, providing full diel coverage. This method does not account for lunar reflectance from either the surface or the aerosol layer. Sensitivity tests do no indicate large systematic or random errors associated with lunar illumination. VIIRS AOT retrievals yield a coefficient of determination (r^2) of 0.60 and a root-mean-squared-error (RMSE) of 0.18 when compared against straddling daytime-averaged AERONET AOT values. Preliminary results suggest that artificial light sources can be used for estimating regional and global nighttime aerosol distributions in the future.

CHAPTER I

INTRODUCTION

Atmospheric Aerosols

Atmospheric aerosol, as defined by the American Meteorological Society (2015a), is "A colloidal system in which the dispersed phase is composed of either solid or liquid particles, and in which the dispersion medium is some gas, usually air." Atmospheric aerosol particles range in size from a few nanometers (nm, 10^{-9} m) to tens of microns (Eck et al., 2003). Atmospheric aerosol particles can be categorized by their principal sources (lifted dust, sea spray, biomass burning, fossil fuels, and secondary organic production) or by their chemical composition (mineral, salt, sulfate, nitrate, black carbon, and organic).

Dust aerosols originate primarily from deserts, specifically the Sahara and those located in the Middle East and Eastern Asia. Long range transportation of dust plumes across the Atlantic and Pacific Oceans is commonly observed (Chin et al., 2007). Smoke aerosols are emitted by burning biomass, such as forests or crops. Major source regions for smoke aerosols are Amazonian South America, Central America, multiple regions in Africa, and the Maritime Continent (Kaufman et al., 2002; Reid et al., 2009). Urban aerosols are primarily composed of carbonaceous and sulfate particles, and are found over major urban areas such as the Eastern United States, Europe, and Southeast Asia (Hegg et al., 1997). Oceanic aerosols, primarily sea salt particles, are produced by bursting oceanic bubbles and sea spray (Kaufman et al., 2002). Concentrations of sea salt aerosols are generally less significant than other

types of aerosols; however the Southern Ocean experiences higher concentrations due to climatologically windier conditions (Smirnov et al, 2009).

The understanding of aerosol optical and physical properties and their spatial and temporal distributions is of an importance to climate studies (Husar et al., 1997). Aerosol particles reflect incoming short-wave radiation from the sun, which has a cooling effect on the Earth's climate (Schwartz et al., 1996). Aerosol particles can also absorb incoming solar radiation and earth emitted long wave energy and, under certain conditions, cause localized warming (Kaufman et al., 2002). The scattering and absorbing of radiation by aerosol particles is known as the aerosol direct effect. Additionally, in order for a cloud droplet to form, an aerosol particle is required on which water can condense — these are called cloud condensation nuclei (CCN; AMS, 2015b). The number of aerosol particles present therefore dictates the availability of CCN, which determines cloud properties and affects precipitation (Rosenfeld et al., 2008). By acting as CCN, aerosol particles indirectly affect climate; this is known as the aerosol indirect effect. Besides climatic impacts, aerosol particles can attenuate radiation and reduce visibility, which is of critical importance to aviation meteorology and military operations (Charlson et al., 1969; Miller, 2003). Global human health is also directly impacted by aerosols, as mortality rates increase under exposure to increased concentrations of aerosol particles, especially for particulate matter with a particle size of less than 2.5 μ m (PM2.5; Pope and Dockery, 2006).

Remote Sensing of Aerosols

Recognizing their importance, scientists have monitored and studied atmospheric aerosol particles through ground-based, in-situ, and satellite observations. One example of a ground-based instrument is a sun photometer. These instruments measure the intensity of incoming sunlight at multiple wavelengths and re-

trieve aerosol properties based on attenuation of sunlight by the atmosphere. A large network of sun photometers comprises the Aerosol Robotic NETwork (AERONET; Holben et al., 1998). The ground-based and in-situ data play a critical role in the observation of the optical and microphysical properties of aerosols, and they provide crucial validation for satellite-based retrievals (Kaufman et al., 1997). The spatial and temporal coverages of in-situ and ground-based measurements are very limited, especially over global oceans.

With their high spatial and temporal coverage, it is desirable to use satellite observations to monitor and characterize the global distribution of aerosol particles. Prominent satellite-based aerosol products today include those from the MODerate resolution Imaging Spectroradiometer (MODIS; Kaufman et al, 1997; Hsu et al., 2004; Remer et al., 2005; Levy et al., 2013), the Multi-angle Imaging SpectroRadiometer (MISR; Diner et al., 1999), the Visible and Infrared Imaging Radiometer Suite (VIIRS; Jackson et al., 2013) and the Cloud-Aerosol LiDAR (Light Detection And Ranging) with Orthogonal Polarization (CALIOP; Winker et al., 2009). CALIOP is an active sensor; this means that the instrument transmits its own radiation and measures backscattered energy (Purkis and Klemas, 2011, pg 19). MODIS, MISR, and VIIRS are passive sensors that rely on radiation from the Earth and Sun for observation. While passive sensors are able to cover significantly more area than active sensors, one glaring weakness in passive sensors is that they are not sensitive to the low levels of visible and near-infrared radiation present at night. Therefore, retrievals cannot be made at night unless sensors designated for nighttime use are implemented.

Nighttime aerosol data are desirable for multiple reasons. Observing aerosol transport at all times is important for monitoring pollution and visibility (Barreto et al., 2013). For example, both military and civilian groups are interested in monitoring aerosol outbreaks that can severely reduce visibility quickly (Zhang et al., 2008b).

Nighttime aerosol data is also important for climatological records, especially in high latitude regions that experience extended periods of time without sunlight (Barreto et al., 2013). As previously mentioned, aerosols impact the Earth's radiation budget; this has been hard to quantify at night due to a lack of aerosol data, especially for climatic impacts on longwave radiation by dust (Zhang et al., 2008b). Finally, Zhang et al. (2014) conducted an extensive aerosol data assimilation study and noted a significant data gap during nighttime. They suggest that assimilation of passively sensed nighttime data could significantly improve model performance.

Currently, quantitative nighttime aerosol data is limited to ground-based photometers and LiDARs, and satellite-based active sensors (Zhang et al., 2008). Star and lunar photometry have been employed in numerous studies (Herber et al., 2002; Berkoff et al., 2011; Perez-Ramirez et al., 2012; Barreto et al., 2013; Baibakov et al., 2015) as a method of retrieving nighttime aerosol optical thickness (AOT, τ). Lanciano and Fiocco (2007) even measured nighttime AOD by taking digital photos of stars with a commercial Nikon D1 Digital Single Lens Reflex (DLSR) camera. However, some issues with star and lunar photometers include signal-to-noise ratio, calibration (Perez-Ramirez et al., 2011), and the lunar irradiance pattern (Barreto et al., 2013). As these instruments are relatively new and very few are deployed, there is currently no large uniformly calibrated and distributed network similar to AERONET (However, this will soon change, as AERONET begins to deploy hybrid sun-sky-lunar photometers [Barreto et al., 2015]). Also, the use of both types of photometers is limited by extremely small spatial coverage (Zhang et al., 2008).

LiDARs, such as the previously mentioned CALIOP, are active sensors that can be ground-based or airborne (Purkis and Klemas, 2011, pg 26). Unlike photometers and passive space-borne sensors, lid can provide the vertical distribution of aerosol data. Ground-based LiDARs such as those in the Micro-Pulse LiDAR Net-

work (MPLNET; Welton et al., 2006) are useful to provide vertical information and other detailed characterization not available from passive instruments (e.g. Campbell et al., 2015); however they experience the same coverage issues as photometers. As CALIOP is space-borne, it is able to cover a significant portion of the globe with a 16-day repeating orbit; however, its small LiDAR footprint limits its coverage (Winker et al., 2009).

Recent Studies

A few previous studies have attempted to quantify night time aerosol properties through passive-based satellite observations. Satellite detection of dust at night has been available since the last century (Legrand et al., 1989; Wald et al., 1998; Miller, 2003; Hansell et al. 2007). This can be as simple as examining the difference between a thermal infrared band ($\sim 11 \mu m$) and a channel around $8.5 \mu m$ (Ackerman, 1997). However, quantification has been more elusive. Hao and Qu (2007) introduced a dust index based on four infrared MODIS bands. Liu et al. (2013) improved upon the brightness temperature difference methods presented in Ackerman et al. (1997) and Wald et al. (1998) to produce a Dynamic Reference Brightness Temperature Difference Index (DRBTDI). Both of these indices performed well (Pearson Correlation Coefficient (r) < 0.78) when compared with CALIOP and MODIS AOT values, respectively. It should be noted that these indices are considered semi-quantitative because they are not directly determining aerosol properties (i.e. AOT is not mathematically derived from the brightness temperature difference used in the indices).

Multiple recent studies (e.g. Han and Sohn, 2013; Wong et al., 2015; Xiao et al., 2015) have presented methods for estimating dust aerosols using Artificial Neural Networks (ANNs). Lee and Sohn (2012) estimated nighttime AOT of dust in Asia by building an ANN. This model was trained by ingesting data that was available

during the day as well as at night, such as various infrared brightness temperatures and surface emissivities and producing a target output of daytime MODIS AOT values. Once the model was trained, nighttime input data was used to produce an estimate of nighttime. This method proved useful for tracking large scale dust events, but the nature of an ANN presents issues. Because the model was trained for dust events over Asia, it may not perform well for different types of aerosols in other parts of the world. Also, since the model was trained to predict MODIS AOT values and, the model will likely have some of the systematic errors that are found in MODIS AOT values.

A more direct method for obtaining nighttime τ via passive remote sensing was presented by Zhang et al. (2008b). This study suggested that changes in magnitude of satellite observed artificial lights (cities) can be explained via attenuation of light by aerosol particles in the atmospheric column. The methodology of this study is as follows. From Beer′s Law (Liou, 2002, pg. 29), the equation for satellite observed radiance can be described as

$$I_{sat} = I_s e^{-\tau}, \tag{1.1}$$

where I_{sat} is the satellite observed Visible Near-Infrared radiance (VNIR; in this study the wavelength range was $0.5\mu m$ – $0.9\mu m$), I_s is the upward radiance at the surface (which includes VNIR radiation from artificial lights and surface reflectance of lunar illumination), and τ is the optical depth of the atmospheric column. Assuming that the atmosphere is cloud-free leaves AOT as the primary contributor to τ. At the time of their study, only the Operational Linescan System (OLS; Elvidge et al., 1999) was available to make VNIR observation at night. Zhang et al. (2008b) note that the OLS was a poor choice for quantitative aerosol data retrievals as it was

not designed for calibrated radiance observation; however, this work was done as a proof of concept with the Suomi National Polar-orbiting Partnership (NPP) satellite (launched in 2011) — housing the new VIIRS Day/Night Band (DNB) — in mind.

The VIIRS DNB (Lee et al., 2006) is the "sequel" to the OLS. The premise is the same — VNIR ($0.5\mu m$ – $0.9\mu m$) observation; however, the VIIRS DNB is a significant upgrade. The OLS was designed for nighttime cloud detection. Its coarse radiometric resolution and lack of calibration leave it largely unsuitable for quantitative studies (Lee et al., 2006). In contrast, the VIIRS DNB was designed to be suitable for quantitative studies — it is calibrated onboard, has a much higher radiometric resolution (13-bit compared to 6-bit for the OLS), and has much less pixel overlap. A list of attributes of the OLS and the VIIRS DNB sensors can be seen in Table 1. These factors allow the DNB to provide detailed, quantitatively robust nighttime radiance data.

As Suomi NPP was launched in October of 2011, Johnson et al. (2013) were able to take advantage of the VIIRS DNB. Expanding on Zhang et al. (2008b), the VIIRS DNB was used to quantitatively estimate AOT by examining the difference between VNIR radiance values from artificial lights and nearby dark pixels. The equation for satellite observed radiance presented in Johnson et al. (2013) is more complicated and more representative of the atmosphere than the equation in Zhang et al. (2008b) as it includes terms for surface reflectance of moonlight, diffuse transmission of moonlight, and a higher order aerosol reflectance term in addition to the artificial light source term; these equations will be discussed further in Chapter 3. The method from Johnson et al. (2013), dubbed the "contrast method", is based on comparing the difference between radiance values for city lights and nearby dark pixels on nights with aerosol present to said difference on an ideal night that is aerosol-, cloud-, and moon-free. They use the cloudless night within the study period with the

Table 1: A list of attributes for the OLS and VIIRS DNB sensors (Miller et al., 2013).

Attribute	OLS	VIIRS DNB
Orbital Details	Sun-synchronus, ∼850km	Sun-synchronus, 824km
Nighttime Nodal Overpass Time	∼1930 UTC	∼0130 UTC
Swath Width	3000 km	3000 km
Spectral Passband Bandwidth	Panchromatic 500–900 nm	Panchromatic 500–900 nm
Spectral Passband Center	∼600 nm	∼700 nm
Horizontal Sampling Interval	2.8 km (Nighttime "smooth" data)	0.740± 0.043 km (Scan) 0.755 ± 0.022 km (Track)
Horizontal Spatial Resolution	5 km (Nadir)/∼ 7 km (Edge)	$<$ 0.770 km (Scan) $<$ 0.750 km (Track)
Geolocation Uncertainty	∼450 m – 5.4 km	266 m (Nadir), 1151 m (Edge)
Minimum Detectable Signal	$4 \times 10^{-5} Wm^{-2} Sr^{-1}$	$3 \times 10^{-5} Wm^{-2} Sr^{-1}$
Noise Floor	$\sim 5 \times 10^{-6} Wm^{-2} Sr^{-1}$	$\sim 5 \times 10^{-7} Wm^{-2} Sr^{-1}$ (Nadir)
Radiometric Quantization	6 Bit	13–14 Bit
Accompanying Spectral Bands	1 (Thermal IR)	11 (Night)/21 (Day)
Radiometric Calibration	None	On-board Solar Diffuser
Saturation, Stray Light Artifacts	Urban Cores, Substantial, Uncorrectable	None, Near-Terminator,Corrected

lowest τ as indicated by daytime AERONET observations as a proxy for an ideal night. Johnson et al. (2013), using interpolated daytime AERONET AOT values as validation, showed that artificial lights can indeed be used to estimate AOT at night with quantitative skill, although they noted many issues and sources of uncertainty, e.g. the instability of the artificial light sources.

The algorithm used in the nighttime aerosol retrieval method of Johnson et al. (2013) is challenging to apply on a global scale for several reasons. First, near identical VIIRS pixels from different nights are needed from a selected artificial light source and the corresponding nearby background. To implement such a method operationally over a large study domain is difficult, as VIIRS DNB viewing geometries vary from day to day. This makes it difficult to select the same group of pixels daily. Second, the inherent variation within an artificial light source, especially for a large city comprised of hundreds of VIIRS pixels, is not considered. Thus, larger retrieval errors may be expected from complex artificial light sources. Third, the contribution from diffused artificial lights needs to be computed, requiring a priori knowledge about aerosol types and aerosol absorbing properties.

In this study, a modification to the Johnson et al. (2013) algorithm is proposed which considers the reduction of radiance contrast of VIIRS DNB pixels within a given nighttime artificial light source as a proxy for aerosol optical depth. This new method overcomes some of the issues encountered by Johnson et al. (2013) and is easier to implement on a global scale. The outline of this thesis is as follows: Chapters II, III, and IV describe the data used in this study, highlight the newly developed approach, and explore the sensitivity of radiance dispersion within a given light source to various parameters, respectively. Chapter V shows the inter-comparisons of the retrieved nighttime AOT from the VIIRS DNB with AERONET and High Spectral

Resolution LiDAR (HSRL) observations. Considerations of uncertainty are included in Chapter VI and Chapter VII summarizes the salient findings of this research.

CHAPTER II

DATA

This study combines VIIRS DNB satellite observations with ground-based sun photometers from four sites in the AERONET network and an HSRL instrument in Huntsville, AL deployed for the National Aeronautics and Space Administration (NASA) Studies of Emissions and Atmospheric Composition, Clouds and Climate Coupling by Regional Surveys (SEAC^4RS) campaign. Table 2 lists the locations, study periods, number of VIIRS AOT retrievals made in this study, and instrumentation at Alta Floresta, Cape Verde, and Grand Forks (the three sites used in Johnson et al. (2013)) as well as a fourth site in Huntsville, AL that is new to this study.

Table 2: Basic information for each of the test sites, including site name, AERONET and HSRL site latitude/longitude locations, and date range of the respective study periods. The "Size of the city" column indicates the number of pixels used in the calculations, which is described in Chapter 3.

Attribute	Site			
	Alta Floresta	Cape Verde	Grand Forks	Huntsville
AERONET Location	9.9°S, 56.1°W	16.7°N, 22.9°W	47.9°N, 97.3°W	34.7°N, 86.6°W
HSRL Location	N/A	N/A	N/A	34.7°N, 86.6°W
Study Period	Aug.–Sep. 2012	Aug.–Nov. 2012	Jun.–Aug. 2012	Jun.–Oct. 2013
# AOT Ret.	18	10	17	20
City Size	50	6	117	509

The VIIRS/DNB Sensor Data Record-SDR (SVDNB) and VIIRS/DNB SDR Geolocation Content Summary (GDNBO) data are used for providing satellite-observed radiance and geolocation values (latitude, longitude, etc.), respectively. The VIIRS DNB observes radiation in a single band with a spectral range from $0.5\mu m$ – $0.9\mu m$, which is considered VNIR. The VIIRS Cloud Cover/Layers Height Data Content Summary (VCCLO) data are used for cloud-clearing of the selected VIIRS pixels. The binary correctness (cloud/no-cloud) of this product at night over land is 90% for cases with an optical depth greater than 1.0 and 85% for cases with an optical depth less than or equal to 1.0 ("Joint Polar Satellite System...", 2011). To mitigate the effects of misclassification by the VCCLO product, VIIRS granules with cloud at any level, as indicated by the VCCLO product, in the vicinity ($\sim 0.1^\circ$ – 0.2° latitude/longitude) of thetarget city are removed. In addition to the calibrated pixel-level top-of-atmosphere radiance values, the VIIRS DNB data products include metadata on satellite and lunar geometry, specifically, satellite, solar, and lunar azimuth and zenith angles, lunar illumination fraction, and quality assurance flags.

For validation purposes, Level 2.0 AERONET data is used in this study. Level 2.0 data has more quality-assurance measures, including removal of cloud-contaminated data (Holben et al., 2006) than previous versions. Level 1.5 AERONET data were chosen in Johnson et al. (2013) as Level 2.0 data were not available for all desired sites during the respective study periods. Updated comparisons between Level 2.0 data and results from Johnson et al. (2013) are included to maintain a consistent comparison between the two studies; however, note that the differences between AERONET Level 2.0 and Level 1.5 AOT values after cloud screening was insignificant. AERONET data at 0.675μm were used in this study, as that is the closest of the AERONET wavelengths to the center of the VIIRS DNB wavelength range, which is between $0.5\mu m$ and $0.9\mu m$.

Nighttime AERONET AOT values are estimated by taking the mean of the daytime AERONET retrievals straddling the VIIRS nighttime overpass (the daytime AERONET AOT values from the evening before the time of the VIIRS overpass and the morning after the time of the VIIRS overpass, as long as both AERONET retrievals are within 24 hours of each other). If, for any reason, there is no available nighttime AERONET AOT estimation, the corresponding VIIRS overpass is not included in this study.

CALIOP nighttime τ data are not used as a validation tool due to a lack of collocated CALIOP and VIIRS data pairs over the selected artificial light sources. Also, recent studies have shown that CALIOP derived AOT values can differ significantly from AERONET (Omar et al., 2013) and MODIS (Ma et al., 2013) values. CALIOP will have a better signal-to-noise ratio for nighttime observations vs. daytime, but Campbell et al. (2012) found that CALIOP AOD had similar errors during both day and night. Even with a perfect CALIOP AOD, the small spatial coverage combined with the long repeat cycle eliminates CALIOP from the list of potential validation tools for this study.

Validating VIIRS nighttime AOT retrievals with daytime AERONET data is not ideal, as the diurnal variation of AOT is a potentially important source of representation error. Thus, nighttime AOT retrievals from the University of Wisconsin HSRL instrument deployed at Huntsville, Alabama (from Jun. 26 – Oct. 26, 2013) are used as an independent validation dataset. Different from CALIOP, HSRL measures both molecular and aerosol backscattering, and thus can be used to derive the ratio of extinction to backscatter (LiDAR ratio), which can be further used to yield a more reliable AOT retrieval (Hair et al., 2008). Besides HSRL measurements, AERONET data are also available for the study period within close proximity to Huntsville, Alabama (UAHuntsville station, 34°N, 86°W). Thus, both Level 2.0 AERONET and

HSRL data from Huntsville, Alabama (from Jun.Oct., 2013) are used in the validation efforts.

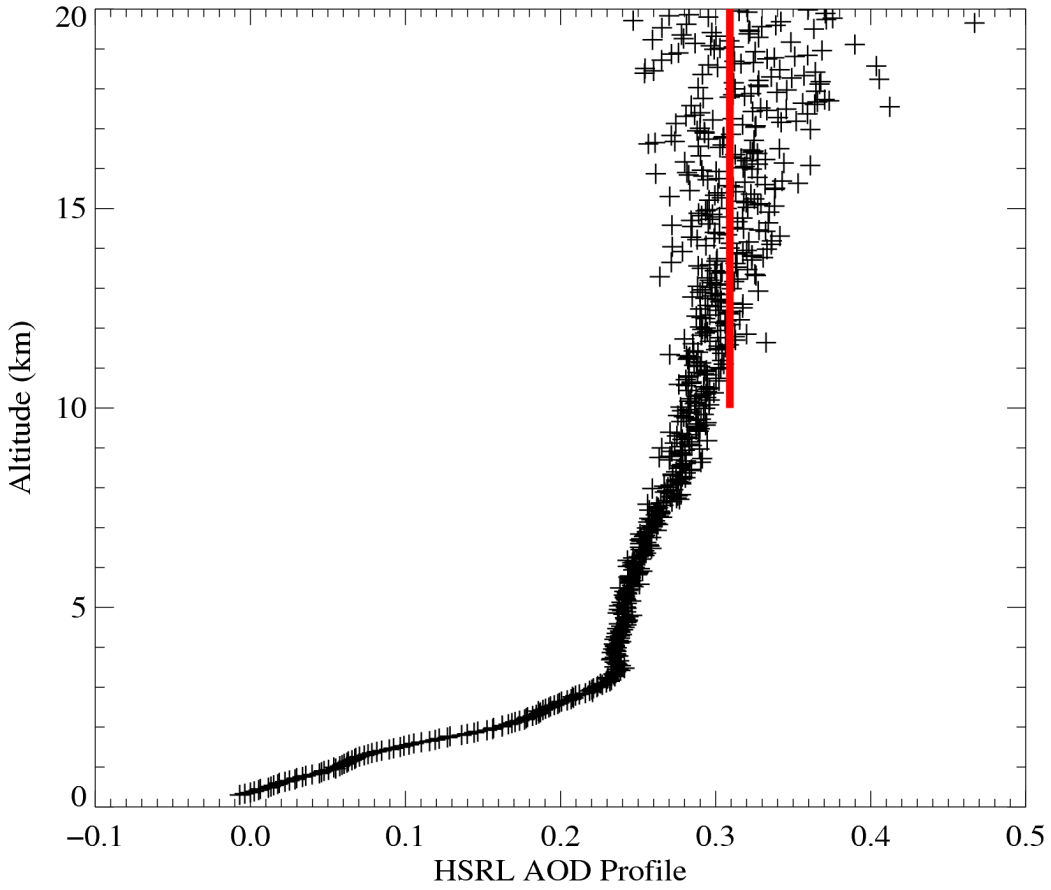

Figure 1: The HSRL AOD profile on 8/25/2013. The total column AOD, found by averaging all values between 10 and 20 km in altitude, is shown in red.

The HSRL data are processed as a ten-minute average at 30 m grid spacing(i.e., each AOT value is the 10 minute average of extinction integrated from the surface up to a given altitude, every 30 m from the surface). Because of noise at higher altitudes, rather than simply taking the column-integrated AOT value at the highest altitude, HSRL total column τ was estimated by taking the average of all column-integrated τ retrievals between altitudes of 10 km and 15 km (Personal communication with Ralph

Kuehn, University of Wisconsin). An example of this can be seen in Fig. 1. HSRL profiles are visually inspected for the presence of clouds, and VIIRS overpasses that occurred on nights with no available HSRL data are not used.

Because the Wisconsin HSRL operates at a wavelength of 0.532 μm, both AERONET observed and VIIRS retrieved AOT values are interpolated to 0.532 μm ($\tau_{0.532}$) using the Angstrom exponent relationship after solving for α:

$$\alpha = -\frac{log\left(\frac{\tau_{\lambda_1}}{\tau_{\lambda_2}}\right)}{log\left(\frac{\lambda_1}{\lambda_2}\right)} \tag{2.1}$$

Here, α is the Angstrom exponent. λ_1 and λ_2 are 0.50 μm and 0.87 μm, respectively. τ_{λ_1} and τ_{λ_2} are the daytime-averaged AERONET AOT values at the respective wavelengths. In order to obtain $\tau_{0.532}$, Eq. 2.1 is rearranged such that

$$\tau_\lambda = \tau_{\lambda_0}\left(\frac{\lambda}{\lambda_0}\right)^{-\alpha}, \tag{2.2}$$

where, in this case, λ is 0.532 μm, λ_0 is 0.675 μm and 0.7 μm (the center of the DNB wavelength range) for AERONET and VIIRS retrievals, respectively, and τ_{λ_0} is the originally retrieved AOT at those wavelengths.

The three sites (Alta Floresta, Cape Verde, and Grand Forks) from Johnson et al. (2013) were originally chosen to represent smoke, dust and, urban cases, respectively. It is important to note that they also vary in spatial extent (6-150 pixels). The Huntsville test site covers a significantly larger area (500 pixels) than the other three sites, allowing for detailed testing of the impact of city size to τ retrievals. Basic information about the four sites examined in this study is found in Table 2.

CHAPTER III

METHODOLOGY

Following Johnson et al. (2013), the satellite observed radiance is composed of three major components, as illustrated in Eq. 3.1:

$$I_{sat} = I_s e^{-\tau/\mu} + D + I_p. \tag{3.1}$$

Here, τ is the total optical thickness, μ is the cosine of the satellite zenith angle, D is the additional diffuse radiance, I_p is the path radiance (i.e. additional radiation reflected and scattered by the atmosphere without interaction with the ground, including aerosol layer reflected moon light), and I_s is the surface upward radiance for an artificial light source. The first term on the right hand side (RHS) of Eq. 3.1 represents the VIIRS observed surface radiance through direct attenuation. The second and the third terms are the diffuse and path radiances, respectively (Johnson et al., 2013). As mentioned in Johnson et al. (2013), I_s can be defined as:

$$I_s = \frac{r_s\big(\mu_0 F_0 e^{-\tau/\mu_0} + \mu_0 F_0 T(\mu_0)\big) + \pi I_a}{\pi(1 - r_s \bar{r})} \tag{3.2}$$

where F_0 is the moon light at the Top of Atmosphere (TOA), μ_0 is the cosine of the lunar zenith angle, r_s is the surface reflectance and $\bar{r}$ is the reflectance from the aerosol layer. T(μ_0) is the diffuse transmittance and I_a is the emission from the artificial light source. The first two terms from the numerator represent reflected direct and diffuse downward moonlight, respectively. Here we assume that emissions from artificial

light sources (I_a) are stable throughout the respective study periods. Also, because pixels comprising a given city are within close proximity, we assume that total optical thickness, diffuse radiance, path radiance, and the reflected direct ($r_s\mu_0 F_0 e^{-\tau/\mu_0}$)) and diffuse ($r_s\mu_0 F_0 T(\mu_0)$) downward moon light are invariant within a given city. Like in Johnson et al. (2013), the $r_s\bar{r}$ term is assumed to be negligible, although this term can be significant for optically thick aerosol plumes. Taking the spatial derivative of Eq. 3.2, and by assuming the D, I_p, $r_s\mu_0 F_0 e^{-\tau/\mu_0}$ and $r_s\mu_0 F_0 T(\mu_0)$ terms are spatially invariant within an artificial light source, yields Eq. 3.3:

$$\Delta I_{sat} = \Delta I_a e^{-\tau/\mu}. \tag{3.3}$$

ΔI_{sat} and ΔI_a are the pixel-to-pixel change in satellite observed radiance and surface emission for a single artificial light source. Solving Eq. 3.3 for τ and introducing a correction term "C" gives Eq. 3.4:

$$\tau = -\mu ln\big(\frac{\Delta I_{sat}}{C\Delta I_a}\big). \tag{3.4}$$

Eq. 3.4 shows that optical thickness can be calculated for a single artificial light source using only the cosine of the satellite zenith angle (μ) and the pixel-to-pixel differences in satellite observed radiance and upwelling radiance from the artificial light source (ΔI_{sat} and ΔI_a, respectively). It is further assumed that the Rayleigh optical thickness is constant regardless of viewing geometry; the error introduced by this assumption is small. C is a correction term applied to account for a dependence of upwelling radiance on satellite viewing angle, which was found to be applicable only at the Grand Forks location as identified from Johnson et al. (2013), due to plausible reasons such as stray light contamination. In Johnson et al. (2013), a linear relationship between cosine viewing angle and VIIRS radiance is constructed, and

for each observation, the C value is estimated by dividing the observed radiance by the radiance value predicted from the linear relationship for the Grand Forks site. C values for Grand Forks have been adopted directly from Johnson et al. (2013) for this study. C is set to 1 for all other sites. A more detailed explanation of this correction term can be found in Johnson et al. (2013). It was suspected that this dependence on viewing geometry was a product of parallax effect, which was corrected with the release of terrain corrected geolocation data (released in early 2014). The difference between terrain-corrected and non-terrain-corrected geolocation data was determined to be sub-pixel in magnitude for Grand Forks. Therefore, the lack of terrain-corrected geolocation for the study periods in this study is not expected to introduce additional error.

As this study intends to examine the radiance contrast between pixels within a given artificial light source, a way to quantify the pixel-to-pixel differences of radiance values within this light source is needed. Although, mathematically, Eq. 3.3 is achieved by taking the spatial derivative of Eq. 3.2, it is beneficial for this method to look at the spatial derivative in the statistical domain. In other words, a measurement of statistical dispersion is used in place of taking the actual derivative. A first check for a signal between dispersion and aerosol loading can be seen in Fig. 2, where, for each retrievable night within the study period, dispersion is plotted against average AERONET AOT. A sensitivity study comparing optical thickness values calculated using each measure of statistical dispersion was also performed. The results from these calculations, after removing dispersion methods based on Fig. 2 are shown in Table 3. These exercises determined that standard deviation produces the best results when compared against AERONET optical thickness values, therefore the Δ operator in Eqs. 3.3 and 3.4 is the "the standard deviation of ...". The sensitivity of τ in

Table 3: Result Statistics for VIIRS AOT retrievals made over Alta Floresta using different methods of dispersion for Δ.

Method	Mean	r^2	RMSE	Slope
Standard Dev.	0.231	0.725	0.107	0.971
Range (all pixels)	0.332	0.724	0.154	1.027
Range (5% removed)	0.042	0.571	0.239	0.982

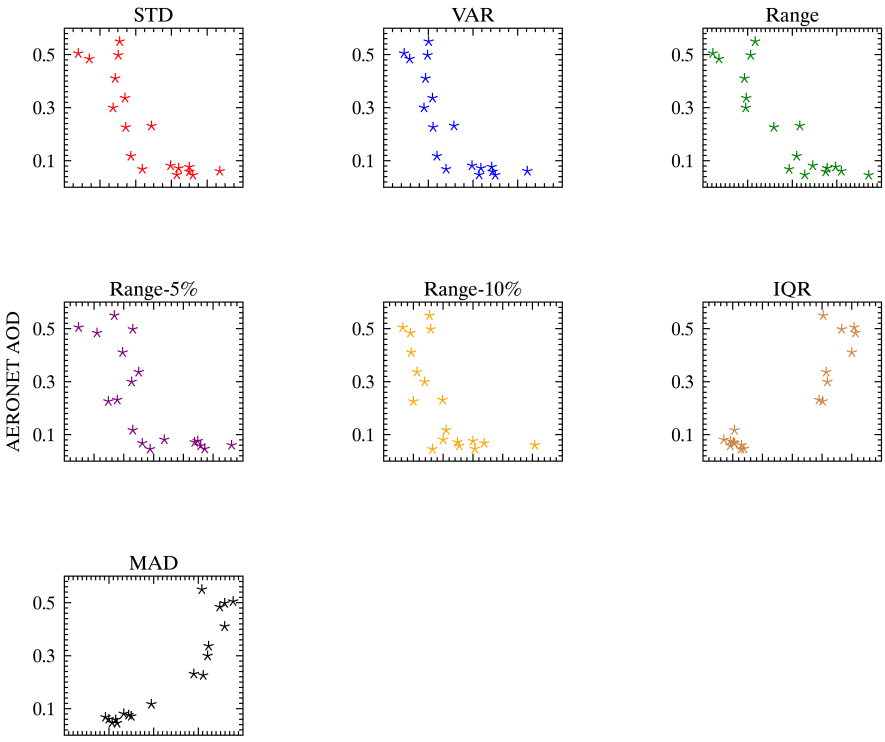

Figure 2: Dispersion values against average AERONET AOT on each potential retrieval night for Alta Floresta. From top left, moving right then down: standard deviation, variance, range, range with the top and bottom 5% of pixels removed, range with the top and bottom 10% of pixels removed, interquartile range, and median absolute deviation. AERONET AOD is on the y-axis and dispersion value is on the a-axis. Units of dispersion are $Wcm^{-2}sr^{-1}$, except in the case of variance, which has units of $(Wcm^{-2}sr^{-1})^2$.

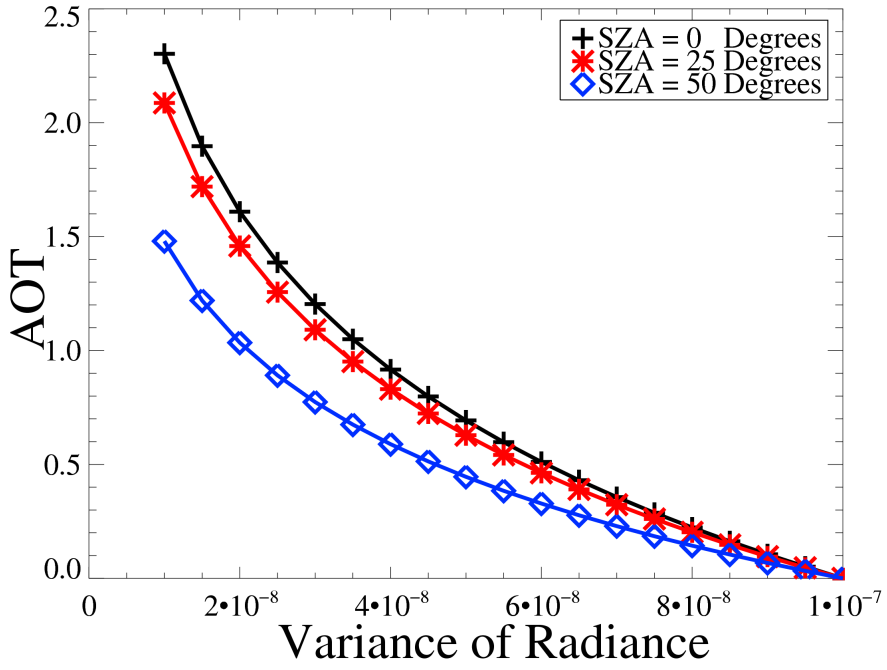

Figure 3: AOT computed by using Eq. 3.4 with varying standard deviations of radiance (ΔI_{sat}, x-axis) and satellite zenith angles, simulating retrievals made using the variation method. ΔI_a is held constant at 10^{-7} $Wcm^{-2}sr^{-1}$.

Eq. 3.4 to varying ΔI_{sat} and satellite zenith angle (with a fixed ΔI_a) is shown in Fig. 3.

The method described above, dubbed the "variance method", is based on radiance values within a given artificial light source; therefore, it is necessary to determine which pixels comprise an artificial light source ("city pixels"). With potential automation in mind, it was decided that city pixels should be determined algorithmically. As suggested from Johnson et al. (2013), any pixel with a radiance value greater than 1.5 times the mean radiance of a given section of a VIIRS DNB granule enclosing the target city, and a radiance value greater than 0.25×10^{-8} $Wcm^{-2}sr^{-1}$ is considered a city pixel. Fig. 4 shows an example of artificial light detected using

this method for Huntsville, Alabama. Because atmospheric conditions, and therefore

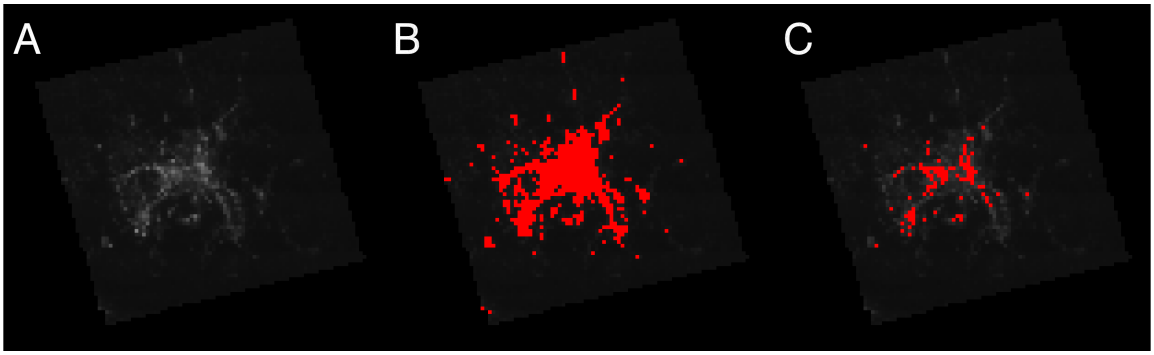

Figure 4: (a). A Raw VIIRS DNB image of Huntsville from the night of June 26th, 2013. (b). The same image from (a) with algorithmically-determined city pixels in red. (c). The same as in (b), except only the 100 brightest city pixels are in red.

VIIRS retrieved radiance values, change on a nightly basis, the number of city pixels for a given city may also change from night to night. In order to remain consistent, n brightest city pixels are used to compute the standard deviation of radiance values for each nighttime VIIRS overpass within the study period of a given city, where n is the minimum number of algorithmically determined city pixels among overpasses that passed VIIRS cloud screening and visual inspection for each city. VIIRS cloud screening is performed by removing any pixels that were flagged as containing cloud at any level in the previously mentioned VCCLO product. Any VIIRS granule of an artificial light source that contains a cloudy pixel in the vicinity of the artificial light source ($\sim$0.2° latitude/longitude) is not used in this analysis.

The only values required to calculate τ from Eq. 3.4 over an artificial light source from a single VIIRS nighttime overpass are ΔI_{sat} and ΔI_a — the standard deviations of radiance values of city pixels from that overpass and the stable (aerosol-, cloud-, and moon-free) standard deviation of radiance values of the city pixels, respectively. The former is straightforward; the latter, however, presents multiple

challenges. First and foremost, a nighttime atmosphere totally free of aerosols and lunar illumination is very unlikely, so error is inherent. Due to the lengths of the VIIRS data record and study periods used for this demonstration, the number of VIIRS overpasses that occur on even nearly aerosol-, cloud-, and moon-free nights within the study periods is extremely limited. It was therefore decided to take ΔI_a for each city as the mean of the two greatest standard deviations of city pixel radiance values within the study period. The rationale behind this is that, in theory, the night with the lowest aerosol loading and least lunar illumination should have the most variance among city pixels. This is not always the case; however, the ΔI_a terms for all locations are taken on nights with τ values below 0.1 (according to the daytime-averaged AERONET τ). A database of VIIRS retrieved radiance values for artificial light sources worldwide is currently being constructed to improve the robustness of this parameter.

Lastly, in contrast to Johnson et al. (2013), only pixels with an artificial light source are needed. It is assumed that the diffuse radiance is spatially and temporally invariant within a given light source, and the derivative is zero. Thus, the newly proposed approach avoids the need for a priori knowledge of aerosol microphysical properties, making it more suitable for a larger scale analysis. This is not to say that differing aerosol optical properties due to different aerosol types will not have an impact on retrievals made via this method; however, the use of a radiative transfer model based on a predetermined aerosol type for each location as in Johnson et al. (2013) is not required to achieve better AOT estimates.

CHAPTER IV

SENSITIVITY STUDIES

The contrast of satellite retrieved radiances within an artificial light source (ΔI_{sat}) is used as the basic information content for the study. It is therefore necessary to examine the impacts of viewing angles and lunar illumination on $\Delta\ I_{sat}$. For example; for a given aerosol loading, do we expect a change in ΔI_{sat} for a moonless night versus a night with significant moonlight? Fig. 5 shows the variance of VIIRS

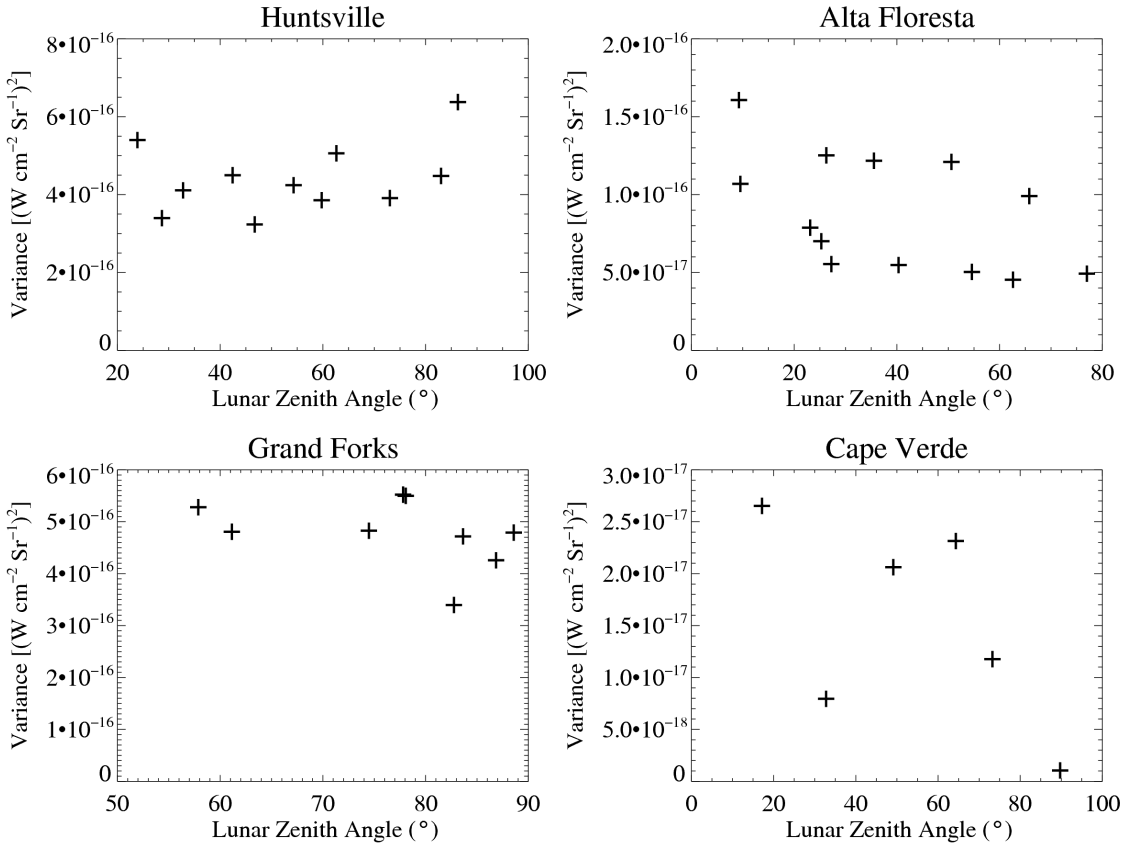

Figure 5: Variance of VIIRS retrieved radiance values versus average lunar zenith angle for each night an τ retrieval was made, separated by location.

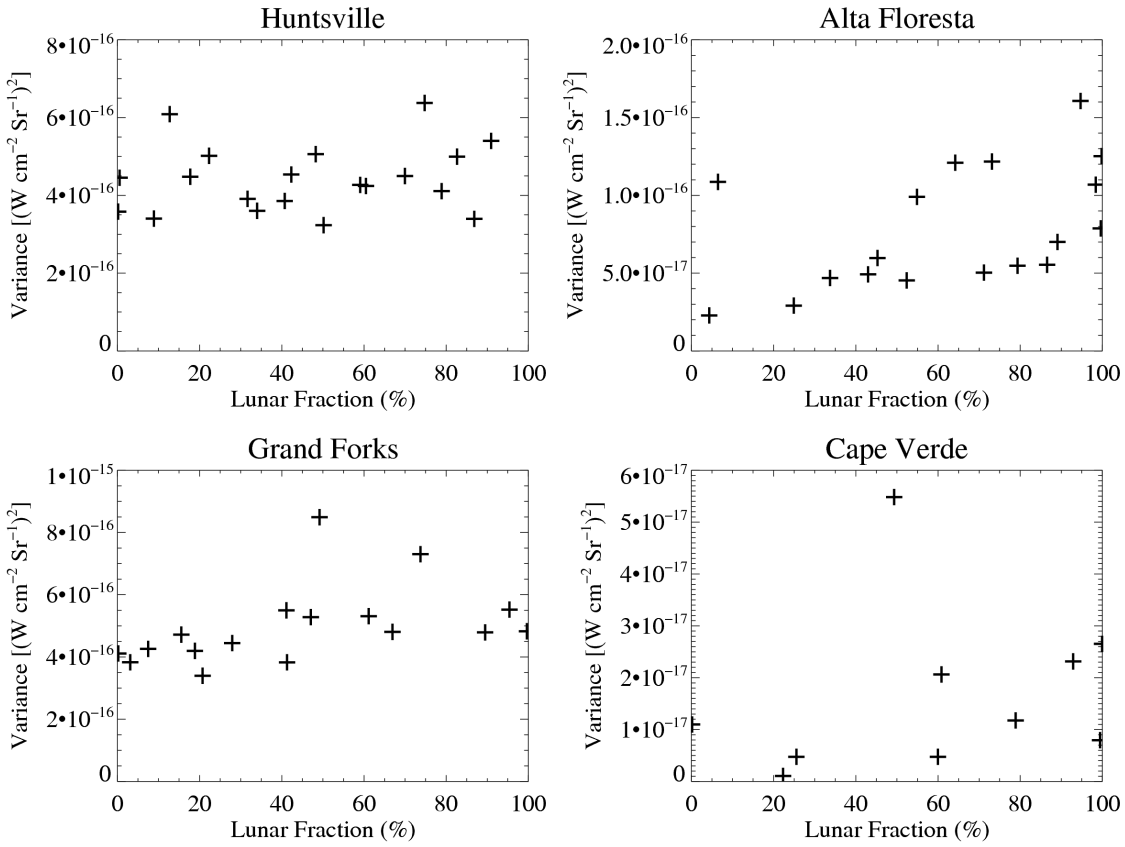

Figure 6: Variance of VIIRS retrieved radiance values versus average lunar fraction for each night an τ retrieval was made, separated by location.

retrieved radiance values of artificial light source pixels plotted against lunar fraction (from the VIIRS GDNBO product). There is a plausible relationship between variance and lunar fraction for the Alta Floresta, Grand Forks, and Cape Verde sites, but the Huntsville site displays no such relationship. This may be due to the fact that the mean radiance for Huntsville is higher than that of Alta Floresta or Grand Forks; however, it is on the same order of magnitude. The Lunar zenith angle (from the VIIRS GDNBO product) was examined in the same manner (Fig. 6), but the data shows no plausible relationship with variance for any location. A variance correction using a linear model was attempted for the three locations showing a potential rela-

tionship, however this correction produced results that are worse than those without the correction, and thus is not used hereafter.

It is anticipated that lunar illumination would introduce a change in ΔI_{sat}. To test this assumption, the ΔI_{sat} values over the Huntsville site are computed for nights with and without lunar illumination that have similar nighttime HSRL τ values. Thus, if the lunar illumination affects ΔI_{sat} under a similar aerosol loading scenario,

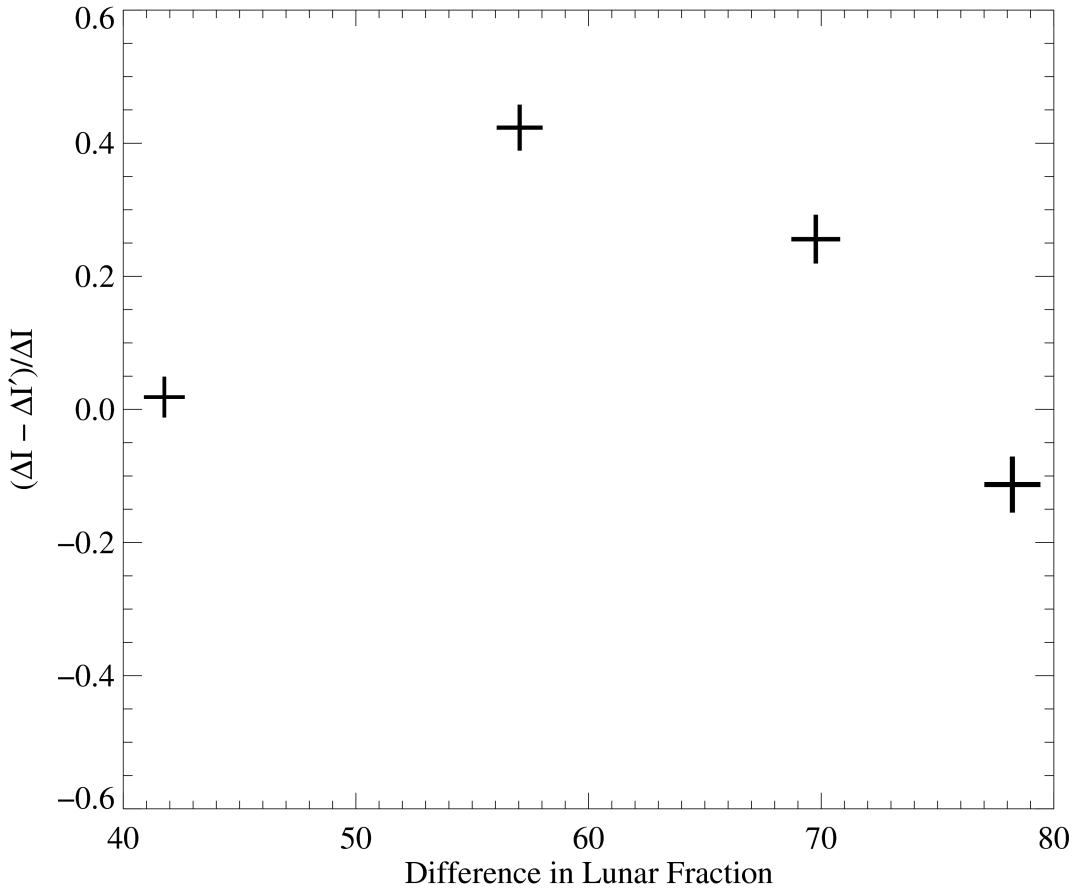

Figure 7: The relative difference in radiance variance for nights with lunar contamination (ΔI on the y-axis label) and without lunar contamination (ΔI'). Each point consists of a pair (one light, one dark) of retrievals with similar (within 0.008) τ. The x-axis indicates the difference in lunar fraction between the paired retrievals. The symbol sizes represent the magnitude of HSRL τ values, which range from 0.15 to 0.25.

a relationship between ΔI_{sat} and lunar fraction should be observed. An examination of the difference in the variance of VIIRS retrieved radiance values between nights with lunar illumination and nights without lunar illumination is shown in Fig. 7. Each data point consists of a pair (one light, one dark) of retrievals with similar HSRL total-column τ (within 0.008 of each other). Also, to minimize the effects of aerosol loading on the derived relationship, only data pairs that have HSRL τ values less than 0.25 (and greater than 0.16, the lowest HSRL τ among retrieval nights) are chosen. The y-axis displays the relative difference in variance for each pair — this is a proxy for the contribution of lunar illumination to the VIIRS τ retrieval. The x-axis is the difference in lunar fraction for each pair. Values of relative contribution range from approximately -.12 (meaning the moonlit night had lower variance) to approximately 0.42. While the sample size is small, this figure displays no clear relationship between lunar fraction and VIIRS radiance dispersion.

Table 4: RMSE of VIIRS retrieved nighttime τ against straddling daytime-averaged AERONET τ for retrievals occurring on nights with (top) and without (bottom) the moon present. Nights with lunar presence are determined as those having a lunar fraction greater than 15% and having a lunar zenith angle less than 89°. The number of retrievals in each category separated by location is also shown.

	Huntsville	Alta Floresta	Grand Forks	Cape Verde	Total	RMSE
Moon present	11	13	8	5	37	0.13
No moon	9	5	9	5	28	0.22

To further test the effects of lunar illumination on the VIIRS retrievals, all retrievals were separated into two groups — those made during which the moon was present and those made without the presence of the moon. Retrievals made in the presence of the moon were determined as all nights having a lunar fraction greater

than 15% and having a lunar zenith angle below 89°. Table 4 shows the root-mean-squared-error (RMSE) of the VIIRS retrieved τ values against daytime-averaged AERONET τ values separated by the presence of the moon, as well as data counts for each subset separated by location. Retrievals were not divided further (such as in Fig. 9) in order to keep the sample size in each subsection sufficiently large and to prevent further locational bias. The RMSE for retrievals made on nights with significant lunar illumination is nearly 0.1 lower than for nights without significant lunar illumination. With this small sample size, lunar illumination cannot be ruled out as a source of retrieval error; however, tests find no evidence for degraded retrieval performance under moonlit conditions.

Similar to Johnson et al. (2013), the relationship between $(\Delta I_{sat})^2$ and viewing geometry is studied. Fig. 8 shows $(\Delta I_{sat})^2$ as a function of satellite zenith angle for Huntsville, Alta Floresta, Grand Forks, and Cape Verde, respectively. Similar to what is reported by Johnson et al. (2013), no viewing angle dependence is found for $(\Delta I_{sat})^2$ for Alta Floresta and Cape Verde. Huntsville also does not display a dependence on viewing geometry. Again, as in the previously mentioned study, a significant positive relationship does exist between $(\Delta I_{sat})^2$ and the satellite zenith angle for Grand Forks. The reason for this relationship, as suggested from Johnson et al. (2013), is still not known and is left to future research once a larger sample size is available.

A major caveat regarding the previously discussed sensitivity studies is sample size. While these sensitivity studies are relatively inconclusive, the study period has not been extended to achieve statistical robustness for several reasons. The first is that cloud screening and HSRL, AERONET Level 2.0, and VIIRS DNB data availability leave little data for analysis. Second, the primary goals of this study are to demonstrate the efficacy of the variance method and to compare the results directly

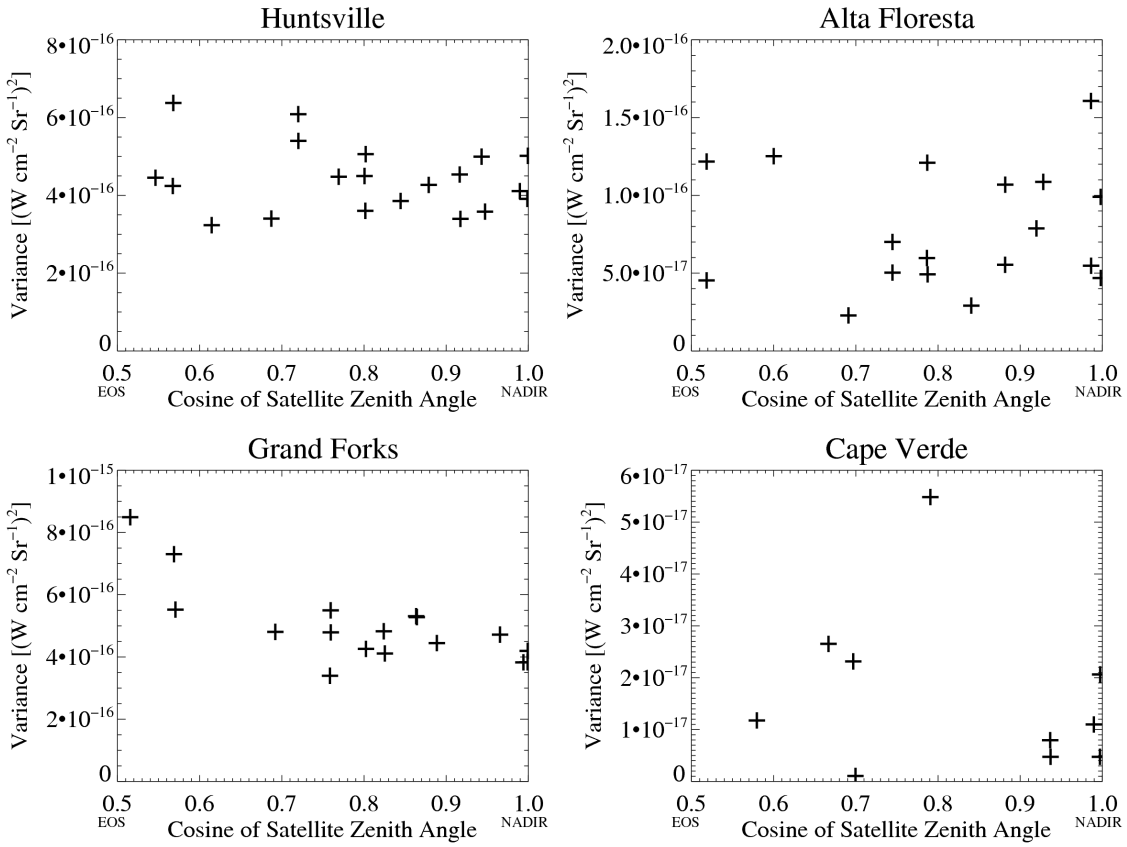

Figure 8: Variance of VIIRS retrieved radiance values versus the cosine of the average satellite zenith angle for each night that a retrieval is made, separated by location. Edge of Scan (EOS) and NADIR are labeled on the x-axis for reference.

with the results presented in Johnson et al. (2013). Third, the short study periods are selected to ensure the relative stability of artificial light sources. For a longer study period, seasonal variations in artificial light sources need to be accounted for, which is beyond the topic of this study and is a subject of future work. Fourth, a regional scale study is underway that will increase the sample size by an order of magnitude; this should be sufficient for conclusions regarding error sources to be made.

CHAPTER V

RESULTS

Validation Against AERONET

For the first step, the VIIRS DNB nocturnally retrieved τ values at 0.7 μm ($\tau_{0.7}$) derived based on Eq. 3.4 are inter-compared with the daytime-averaged AERONET τ at 0.675 μm ($\tau_{0.675}$) values. Fig. 9a shows VIIRS retrieved $\tau_{0.7}$ values

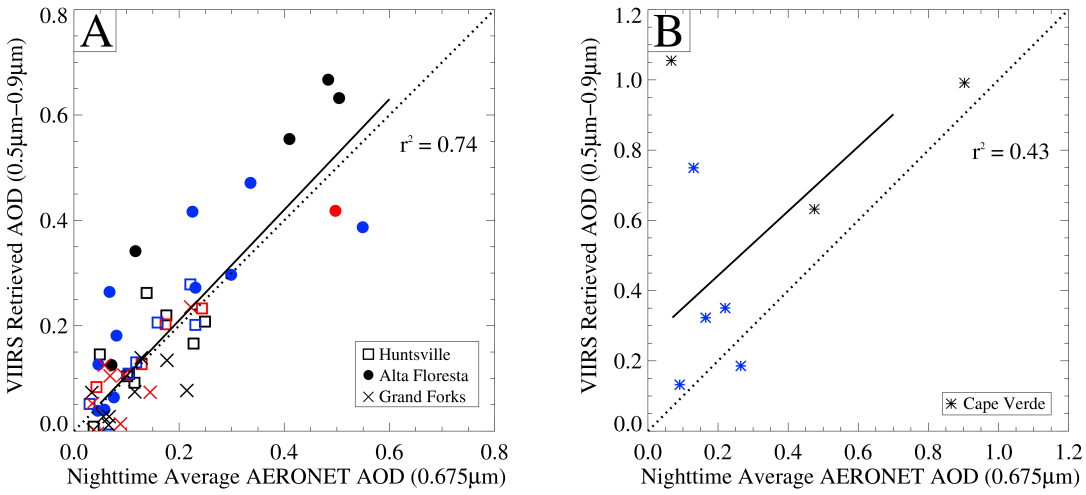

Figure 9: VIIRS retrieved τ as a function of daytime-averaged AERONET τ for Huntsville (left, Figure 9a, square), Alta Floresta (left, Figure 9a, circle), Grand Forks (left, Figure 9a, "x"), and Cape Verde (right, Figure 9b, asterisk). One-to-one (dotted) and best-fit (solid) lines are also shown. Cape Verde is isolated due to its relative small size (6 pixels). Retrievals made on nights with a lunar fraction less than 15% or with a lunar zenith angle greater than 89° (below the horizon) are shown in black. Retrievals made on nights with a lunar fraction greater than 15% but less than 504% and a lunar zenith angle less than 89° are shown in red. Retrievals made on nights with a lunar fraction greater than 50% and a lunar zenith angle less than 89° are shown in blue.

plotted against the corresponding daytime-averaged AERONET $\tau_{0.675}$ for Huntsville (square), Alta Floresta (circle), and Grand Forks ("x"). Cape Verde (Fig. 9b, asterisk) is isolated, as it is comprised of significantly fewer pixels than the other locations. It is suspected that the cause of the poor performance of the VIIRS τ retrievals over Cape Verde is due to the inherent weakness in calculating standard deviation with such a small sample size. This issue is further explored in Chapter VI. The coefficient of determination (r^2) of the VIIRS retrieved nighttime $\tau_{0.7}$ for all locations and daytime-averaged AERONET $\tau_{0.675}$ is 0.60, with a RMSE of 0.18. The r^2 values for Huntsville, Alta Floresta, Grand Forks, and Cape Verde are 0.63, 0.72, 0.38, and 0.43, with RMSEs of 0.04, 0.13, 0.06, and 0.40, respectively. It is noted that because ΔI_a (the "stable" upwelling radiance from the artificial light source) for each city is taken from the average of two nights within the study period as explained above, there is one VIIRS τ retrieval for each location that is at or below 0, which is not physically possible, and one VIIRS τ retrieval slightly above 0. These retrievals were not removed for the calculations of r^2, RMSE, or best-fit lines, and negatively impact the results.

One of the main purposes of this study is a comparison between the "variance method" developed here and the method presented in Johnson et al. (2013, hereafter "background method"). r^2, RMSE, and best-fit slope of nighttime $\tau_{0.7}$ retrievals made using the variance method and nighttime $\tau_{0.7}$ retrievals made using the background method (Table 5, Johnson et al., 2013) compared against the corresponding daytime-averaged AERONET $\tau_{0.675}$ values are shown in Tables 5 and 6, respectively. Huntsville data is not included in Table 5, as it is not reported in Johnson et al. (2013). For Alta Floresta (moderate aerosol loading, moderate size), the variance method performs better than the background method in all statistics. For Grand Forks (low

Table 5: Coefficient of determination, root-mean-squared error (RMSE), and best-fit slope of VIIRS estimated nighttime τ compared against estimated nighttime Level 2.0 AERONET τ at the three original locations for the new method presented in this study. Average AERONET τ for each location is provided for context.

Location	r^2	RMSE	Slope	Mean AOT
Alta Floresta	0.72	0.13	0.96	0.23
Grand Forks	0.38	0.06	0.61	0.10
Cape Verde	0.43	0.40	0.92	0.32
Huntsville	0.63	0.04	0.88	0.14

Table 6: Coefficient of determination, root-mean-squared error (RMSE), and best-fit slope of VIIRS estimated nighttime τ compared against estimated nighttime Level 2.0 AERONET τ at the three original locations for the new method presented in Johnson et al. (2013). Average AERONET τ for each location is provided for context.

Location	r^2	RMSE	Slope	Mean AOT
Alta Floresta	0.60	0.16	1.07	0.23
Grand Forks	0.33	0.05	0.51	0.10
Cape Verde	0.86	0.13	0.81	0.32
Huntsville	N/A	N/A	N/A	N/A

aerosol loading, large size), the methods perform comparably. It is suspected that the poor performance of both methods over Grand Forks is due to the very low aerosol loading and relatively high error inherent in these methods. For Cape Verde (high aerosol loading, very small size), the background method performs significantly better than the variance method. Based on these results, it is hypothesized that the background method performs better for smaller or more isolated artificial light sources and the variance method performs better for larger artificial light sources.

This hypothesis will be furthered investigated once a large scale analysis has been performed.

Validation Against HSRL

The variance method is further evaluated with the use of HSRL data over Huntsville. Fig. 10a shows VIIRS retrieved $\tau_{0.7}$ values interpolated to 0.532 μm ($\tau_{0.532}$), plotted against the corresponding time-averaged HSRL retrieved total-column $\tau_{0.532}$ values for Huntsville. The r^2 of the interpolated VIIRS retrieved nighttime $\tau_{0.532}$ values and averaged HSRL retrieved total-column $\tau_{0.532}$ values is 0.48, with a RMSE of 0.08 (with a mean HSRL τ of 0.25, for context), indicating that the VIIRS-based nighttime τ retrieval method has some skill. Also, daytime-averaged AERONET $\tau_{0.532}$ (interpolated to $0.532\mu m$) is plotted versus the averaged HSRL $\tau_{0.532}$ values as

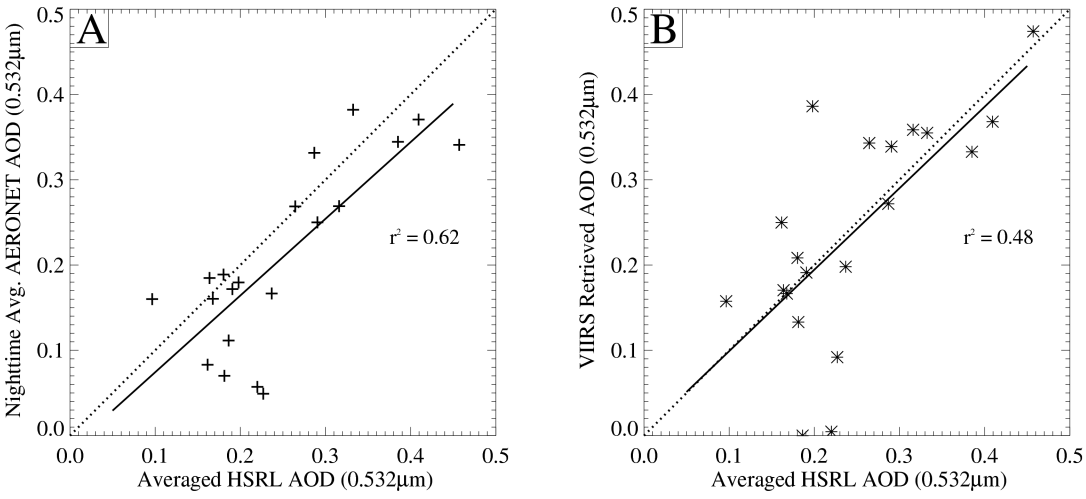

Figure 10: Daytime-averaged AERONET τ_{532} (Figure 10a) and VIIRS retrieved τ_{532} (Figure 10b) as a function of Wisconsin HSRL retrieved total-column τ for Huntsville, Alabama. One-to-one (dotted) and best-fit (solid) lines are also shown.

shown in Fig. 8b. Clearly, Fig. 10b suggests there is value to using the average of the "bookend" daytime AERONET τ observations as a nighttime validation tool when there is a lack of better options. Figs. 9 and 10 show that, while far from perfect, the method presented in this study has some skill at capturing variations in nighttime τ.

To further investigate the effects of lunar illumination on the VIIRS τ retrievals, relative errors (VIIRS retrieval, interpolated, minus HSRL total-column, divided by HSRL total-column τ) for the Huntsville retrievals are plotted as a function of HSRL total-column τ as shown in Fig. 11. The lunar fraction (a percentage

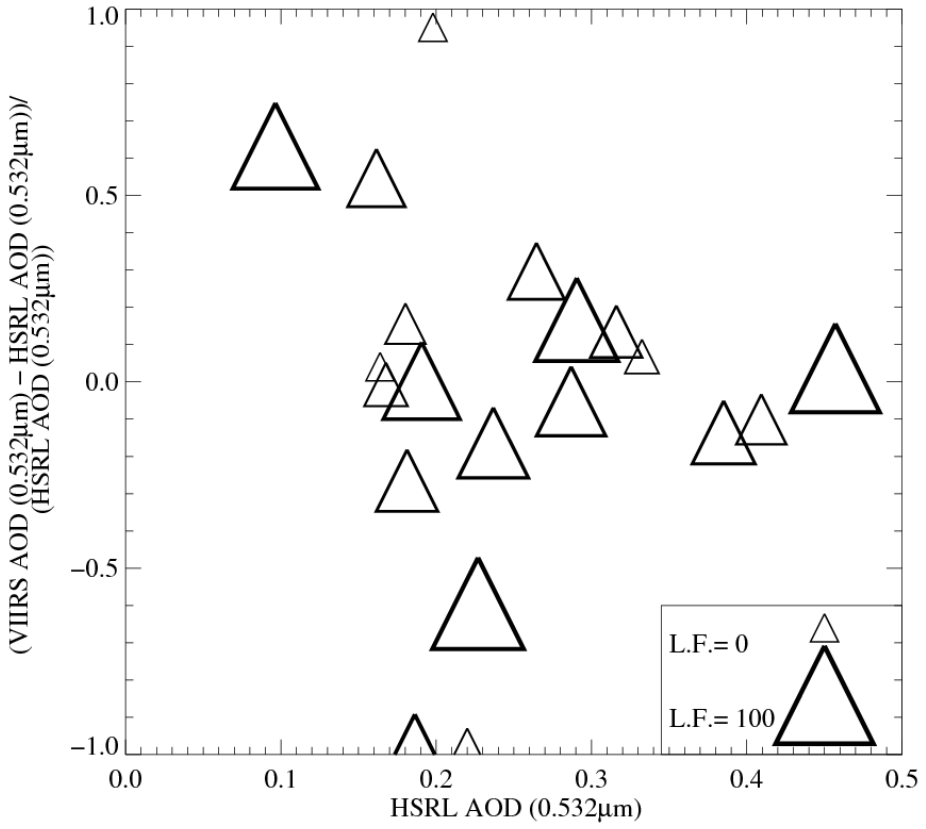

Figure 11: Relative error of each VIIRS τ retrieval (interpolated to 0.532m) with respect to HSRL retrieved total-column τ , plotted as a function of the HSRL retrieval. The Lunar Fraction (0-100%) is indicated by plot symbol size, as shown by the key in the bottom right corner.

from 0-100) on the night of the retrieval is indicated by the plot symbol size. This figure shows that there is no apparent relationship between retrieval error and lunar fraction. It is clear from Fig. 11, however, that the relative error of the VIIRS retrievals decreases as HSRL total-column τ increases (the magnitude of the error [y-axis] goes to zero moving right on the x-axis), as expected. This indicates that VIIRS retrievals are more accurate for aerosol loading events with τ greater than approximately 0.25.

Because this method performs the worst for Cape Verde (the smallest city by number of pixels), a sensitivity study is performed for Huntsville, Alta Floresta, and Grand Forks to determine if the number of "city pixels" used in the retrieval is an important factor for its quality. Cape Verde is not used because reducing the already small number of pixels produces results that are not robust. To achieve this goal, the relationship between the number of artificial city light pixel using in the VIIRS τ retrievals to the ΔI_{sat} values are studied over relative aerosol free nights (HSRL and/or AERONET τ less than 0.2, see Table 7). For each location, the n brightest

Table 7: Dates with HSRL (for Huntsville) or daytime-averaged AERONET (Grand Forks and Alta Floresta) τ less than 0.2, which are used for the computations shown in Fig. 12, and the baseline (i.e. used in the actual τ retrieval) n pixels used for Grand Forks, Huntsville, and Alta Floresta

Location	Year	Dates with less than 0.2 AOT	Baseline n pixels
Grand Forks	2012	6/12, 6/15, 6/21, 6/26, 6/29, 7/3, 7/9, 7/11, 7/14, 7/18, 7/19, 7/23, 7/24, 7/26, 7/27, 7/30, 7/31	117
Huntsville	2013	7/13, 7/19, 8/2, 8/25, 8/26, 8/27, 8/29, 9/5, 9/11, 9/22, 9/27, 10/4, 10/8, 10/11, 10/14	509
Alta Floresta	2012	8/2, 8/3, 8/4, 8/5, 8/7, 8/8, 8/9, 8/15	50

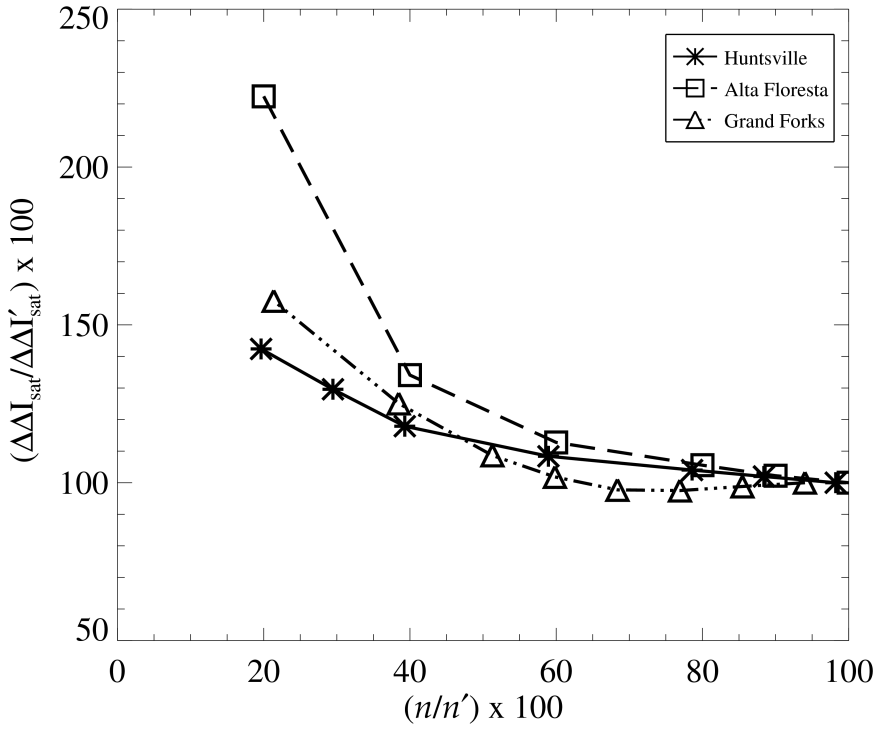

Figure 12: The normalized standard deviation of ΔI_{sat} values ($\Delta\Delta I_{sat}$) as a function of the normalized number of brightest artificial city light pixels (n) for selected nights that are relatively aerosol free (HSRL and/or AERONET $\tau < 0.2$) for Huntsville, Alta Floresta, and Grand Forks. For a given location and for a given number of brightest artificial city light pixels taken from among the baseline case pixels, the standard deviation of ΔI_{sat} values are first computed using data from selected relative aerosol free nights. Both n and $\Delta\Delta I_{sat}$ value are then normalized based on the values used in the actual retrievals (n', $\Delta\Delta I'_{sat}$) as shown in Figures 9 and 10 (details are listed in table 7) for a comparison among different locations.

pixels of the original algorithmically determined city pixels (i.e. the data that are used to create Figs. 9 and 10, also included in Table 7) are treated as the baseline of the study. For a given location, ΔI_{sat} values are computed for the identified relatively aerosol free nights using the baseline defined number of brightest artificial light pixels. Then, a standard deviation of ΔI_{sat} values ($\Delta\Delta I_{sat}$) is computed. $\Delta\Delta I_{sat}$ represents the relative stability of ΔI_{sat} values used in the VIIRS τ retrievals. Next, we repeat the process by incrementally reducing the number of artificial light pixels used in the

analysis. For example, we reduce the number of pixels used for a Huntsville retrieval to 400 (as opposed to the original 509 pixels used) by taking the 400 brightest pixels out of the original 509 pixels. ΔI_{sat} is then computed for each night in Table 7 with the 400 brightest pixels treated as the artificial light source.

The result of the exercise is shown in Fig. 12. The x-axis is the number of brightest artificial light pixels used in computing $\Delta\Delta I_{sat}$ normalized by the number of pixels used in the actual retrieval for each respective location (see Table 7). The y-axis is $\Delta\Delta I_{sat}$ normalized by the $\Delta\Delta I_{sat}$ from the baseline cases. It is clear from Fig. 12 that the normalized $\Delta\Delta I_{sat}$ increases as the number of pixels used in the retrieval decreases. This increased variability translates into a less reliable retrieval. It is hypothesized that this is because standard deviation as a quantification of statistical dispersion is more robust as the sample size increases. Therefore, it is suggested that only medium to large cities (on the order of 10s of VIIRS pixels in spatial coverage at least) are used for nighttime retrievals via the method outlined in this study; however, an exact size has yet to be determined and is a topic left for future studies.

CHAPTER VI

UNCERTAINTIES AND LIMITATIONS

Similar to Johnson et al. (2013), by taking the total derivative of Eq. 3.4,

$$d\tau = \mu\left(\frac{dC}{C} + \frac{d\Delta I_a}{I_a} - \frac{d\Delta I_{sat}}{\Delta I_{sat}}\right); \tag{6.1}$$

thus, the uncertainty in the estimated VIIRS τ is a combined relative uncertainty from the correcting factor C (only applied to Grand Forks), as well as relative errors in the standard deviation of satellite radiance and surface outgoing radiance within an artificial light source, weighted by cosine of viewing angle. For example, a 10% error in the derived ΔI_s could introduce an error in VIIRS τ of 0.05 at the viewing angle of 60° (μ=0.5), and at nadir, the retrieved error increases to 0.1.

There are major issues that need to be explored that could potentially limit implementation of the research presented in this paper. For example, ΔI_a, which is the surface artificial light source emission, is assumed to be invariant through the study period. However, ΔI_a may, and almost certainly does, change with time and viewing geometry (Roman and Stokes, 2015). Even with a constant satellite zenith angle, viewing direction could present an additional issue, especially when viewing artificial light sources. This is because complex surfaces such as cities are likely less Lambertian than other surface, which could mean reflected light is a function of the direction from which (not just the angle) the city is viewed.

Thus, to fully investigate this problem, a careful analysis of the spatial and temporal variations of artificial light sources is needed. Also, the uncertainties at the

low and high AOD ranges could be dominated by different factors. In a high AOD regime, the ignored $r_s\bar{r}$ term can be significant. In a low AOD regime, however, the $r_s\bar{r}$ term can be ignored, while the ignored Rayleigh optical depth can be comparable in magnitude to the retrieved AOT. Other currently unresolved factors related to the artificial light sources that may introduce uncertainty include an unexpected increase in the artificial light emissions (e.g., a large scale fire event). In this study, city pixels are determined algorithmically using purely radiance values, which means that the exact same locations on the earth were not necessarily chosen for each retrieval. While there may be a way to implement official boundaries into determining which pixels are city pixels, cities often do not simply end at boundaries. These sources of uncertainty are in addition to previously mentioned relationships due to lunar and satellite variables.

Cloud contamination is likely to be another major source of uncertainty. With only limited visible and infrared channels, nighttime cloud, and especially thin cirrus cloud, detections may be problematic. Since this is a case study, all VIIRS granules are visually inspected. However, to fully automate the process, additional cloud screening checks will most likely be needed, which will require the use of other VIIRS channels or data from other sensors.

CHAPTER VII

CONCLUSIONS

This study presents a new method for using radiance values observed by the Visible/Infrared Imaging Radiometer Suite (VIIRS) Day/Night Band (DNB) over artificial light sources to estimate nighttime aerosol optical thickness (τ). This method is based on theoretical radiative transfer equations for the retrieval of optical thickness using contrast reduction of radiances from artificial light sources within a close proximity. This study seeks to improve upon the shortcomings inherent in the method presented by Johnson et al. (2013) and build toward a method that can be implemented in an automated system. This study suggests:

- Compared with the method of Johnson et al. (2013), the new method shows overall improved agreement between VIIRS DNB nighttime τ and nighttime τ values estimated from AErosol RObotic NETwork (AERONET) and High Spectral Resolution LiDAR (HSRL) measurements.

- A reasonable agreement is also found between nighttime HSRL τ values and interpolated nighttime AERONET τ values that are approximated based on daytime AERONET data. Thus, daytime AERONET τ observations can be used semi-quantitatively as validation for nighttime τ retrievals when other options are not present. The proposed algorithm has significant limitations. Expected uncertainties arise from lunar illumination, viewing geometry, and city characteristics. Various tests described in this study did not show any systematic impact of lunar illumination on the retrieval, but the small sample

size prevents drawing strong conclusions from this. Also, to implement the algorithm in a regional or global analysis, an automated cloud screening scheme is needed to take the place of the manual cloud screening performed in this study.

- While it is expected that lunar illumination has an effect on the retrievals presented in this study, the magnitude of contribution to retrieved τ values from lunar contamination is unclear. For example, data from the largest artificial light source (Huntsville), which has coincident nighttime HSRL measurements, display no relationships between lunar fraction and VIIRS retrieved τ values, relative error, or variance of radiance values.

An operational nighttime aerosol product from a passive remote sensing method is still non-existent. The Cloud-Aerosol LiDAR with Orthogonal Polarization (CALIOP) does provide nighttime aerosol measurements, but the coverage of the non-scanning CALIOP observations is very limited (a single track roughly 70m across). This limits the use of CALIOP data in aerosol modeling and forecasts. This study presents a novel technique for deriving nighttime aerosol properties from the VIIRS that, despite important limitations, shows skill in comparison with ground based measurements. The methods described here will lead to future improvements in developing a reliable nighttime aerosol product for the aerosol modeling community.

APPENDICES

Appendix A
List of Abbreviations

Table 8: List of Abbreviations

Abbreviation	Full Text
AERONET	AErosol RObotic NETwork
ANN	Artificial Neural Network
AOT	Aerosol Optical Thickness
CALIOP	Cloud-Aerosol LiDAR with Orthogonal Polarization
CCN	Cloud Condensation Nuclei
DNB	Day/Night Band
DRTDBI	Dynamic Reference Brightness Temperature Index
DSLR	Digital Single-Lens Reflex
GDNBO	VIIRS/DNB SDR Geolocation Content Summary
HSRL	High Spectral Resolution LiDAR
LiDAR	Light Detection and Ranging
MISR	Multi-angle Imaging Spectroradiometer
MODIS	MODerate resolution Imaging Spectroradiomter
MPLNET	Micro-pulse LiDAR NETwork
NASA	National Aeronautics and Space Administration
NPP	National Polar-orbiting Partnership
OLS	Operational Line Scan
r2	Coefficient of determination
RMSE	Root-Mean Squared Error
SEAC^{4}RS	Studies of Emissions and Atmospheric Composition, Clouds, and Climate Coupling by Regional Surveys
SVDNB	VIIRS/DNB Sensor Data Record-SDR
VCCLO	VIIRS Cloud Cover/Layers Height Data Content Summary
VIIRS	Visible-Infrared Imaging Spectroradiometer
VNIR	Visible and Near-Infrared Radiation

Appendix B
Distribution of Radiance Values

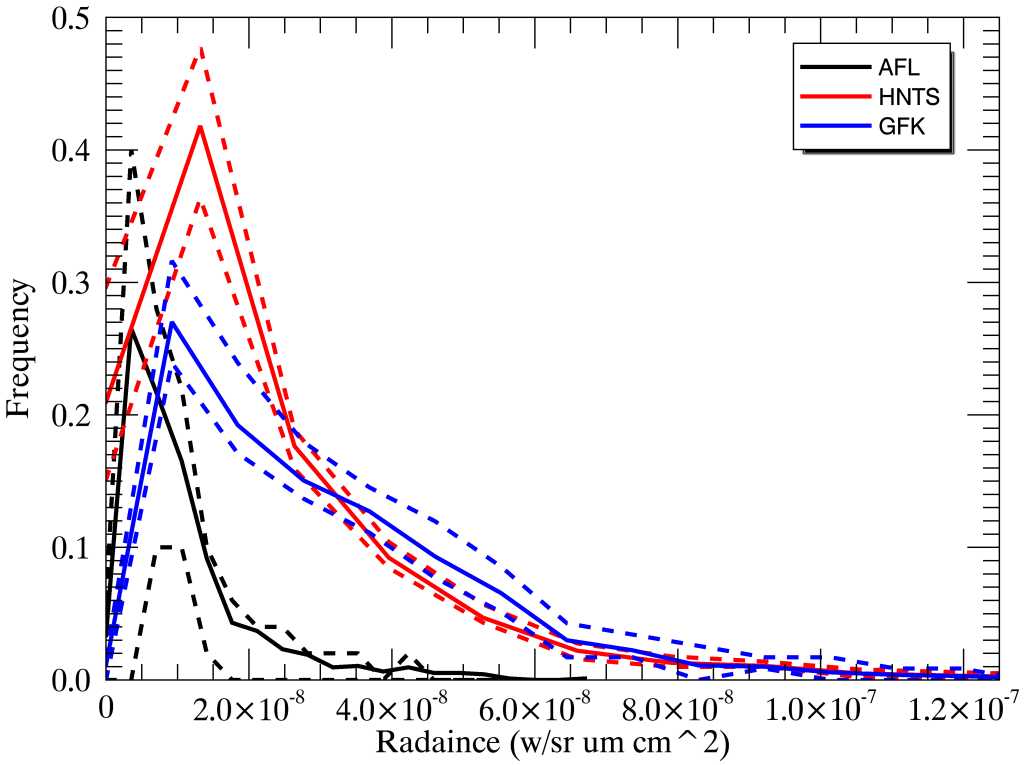

Figure 13: Average PDF for Radiance of City Pixels for Alta Floresta, Huntsville, and Grand Forks. Dotted lines indicate the 25th and 75th percentiles of each bin. The non-Gaussian distribution of radiance values suggests that a measure of dispersion that is more robust under skewed conditions may be worth investigating.

Appendix C
Grand Forks Viewing Geometry

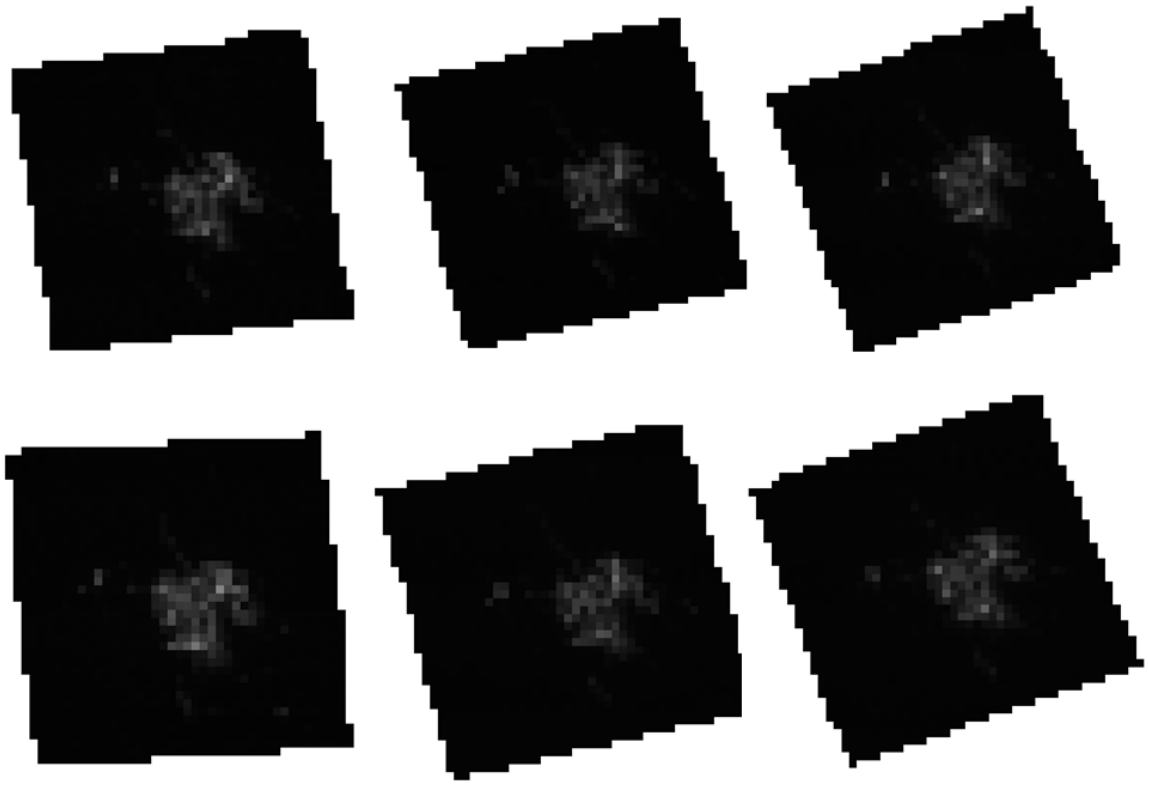

Figure 14: Raw VIIRS DNB Images of Grand Forks under Different Viewing Geometries. There are two images where Grand Forks is left of NADIR (top left, bottom left), two images where Grand Forks is near NADIR (top center, bottom center), and two images where Grand Forks is right of NADIR (top right, bottom right). Satellite zenith angles are displayed under each image.

Appendix D
Cape Verde Outlier

A significant outlier among VIIRS AOT estimates occurred over Cape Verde on October 23rd, 2012; the average AERONET AOT was 0.067, while the VIIRS estimated AOT was over 1.0. The VIIRS DNB image of Sal Island during this overpass, with Espargos (the location of the AERONET site and the VIIRS retrieval) circled in red, is shown in Fig. 15. This image is not significantly different than VIIRS DNB images from other overpasses during which retrievals were made. The VIIRS M16 Band (11.54m 12.49m) is shown in Fig 16. Cloud is clearly visible in this image (regions of blue and green); however, it is approximately 50 miles south of Sal Island. A basic nighttime cirrus test (Ackerman, 1997) is performed by taking the difference between VIIRS M12 Band (3.6m 3.79m) and the VIIRS M15 Band (10.26m 11.26m) and is shown in Fig. 17. Neither VIIRS M Band image indicates cloud over Sal Island, though both images were re-gridded out of necessity. Also note that thin cirrus can go undetected by most basic cloud detection techniques. It is therefore still unknown why the variance method performed so poorly on this night.

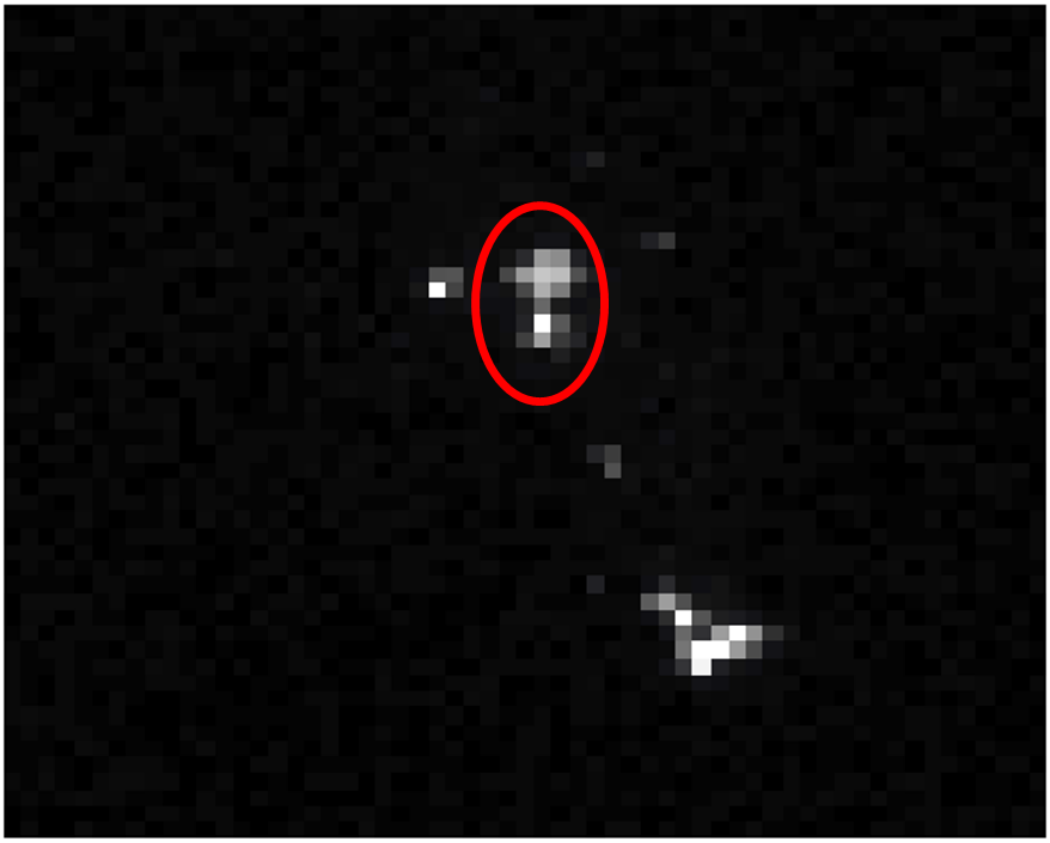

Figure 15: Raw VIIRS DNB Image of Sal Island, Cape Verde, on October 23rd, 2012. Espargos is circled in red.

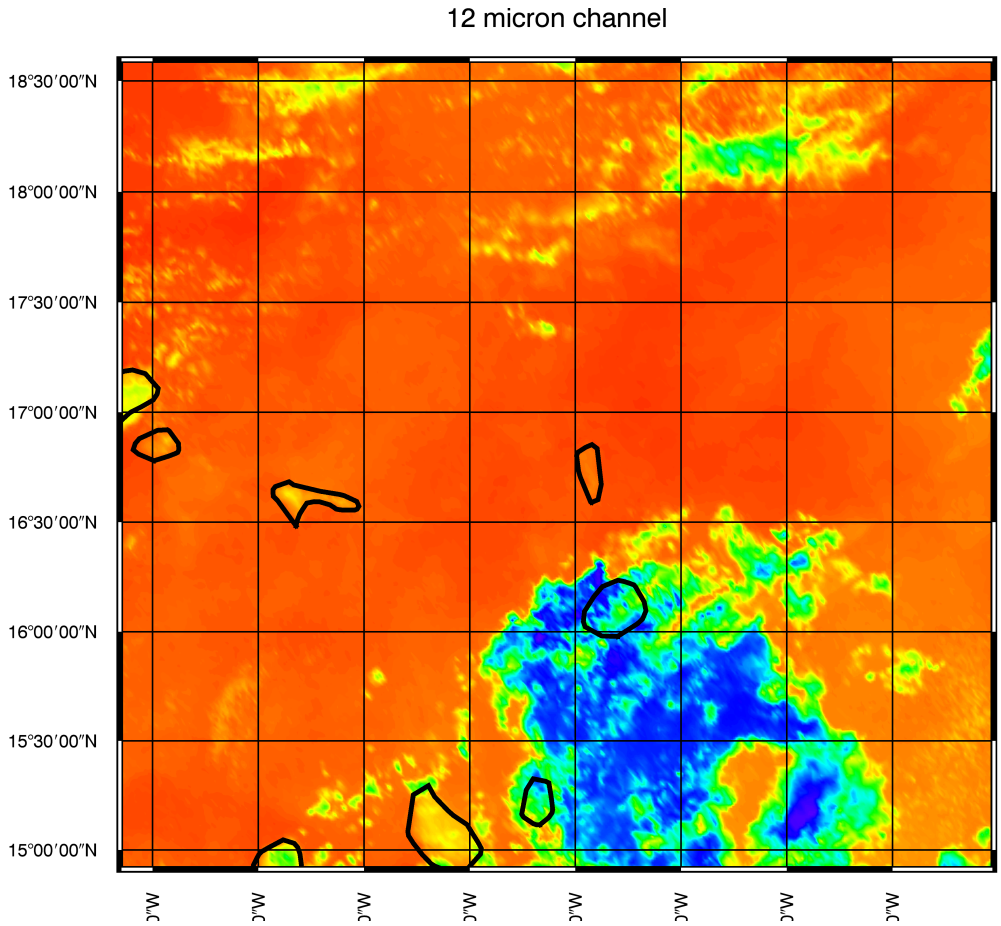

Figure 16: 12 Micron Channel Image over Cape Verde on October 23rd, 2012. Sal Island is located in the center of the image.

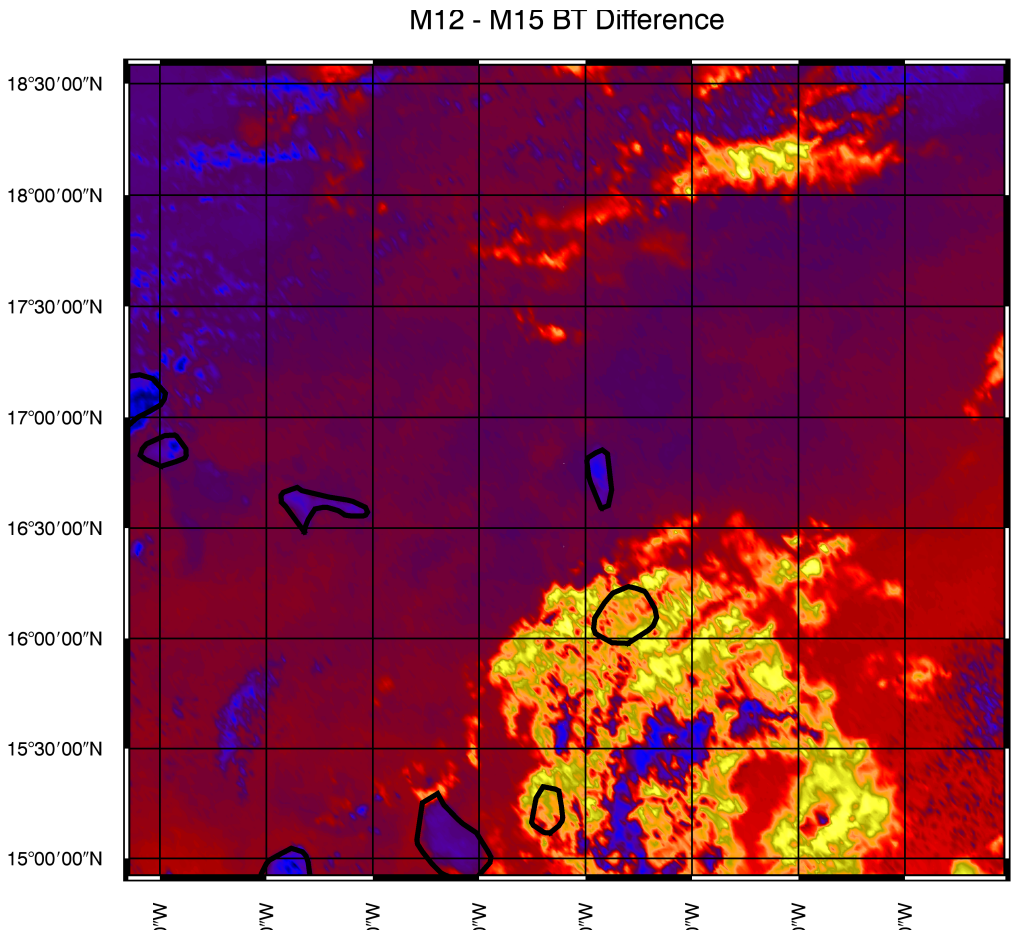

Figure 17: Difference Between M12 Band and M15 Band over Cape Verde on October 23rd, 2012. Sal Island is located in the center of the image.

REFERENCES

Ackerman, S. A. (1997). Remote sensing aerosols using satellite infrared observations. Journal of Geophysical Research: Atmospheres (19842012), 102(D14), 17069-17079.

American Meteorological Society, cited 2015: "aerosol". Glossary of Meteorology. [Available online at http://glossary.ametsoc.org/wiki/"aerosol"]

American Meteorological Society, cited 2015: "Cloud condensation nuclei". Glossary of Meteorology. [Available online at http://glossary.ametsoc.org/wiki/"Cloud_condensation_nuclei"]

Baibakov, K., O'Neill, N. T., Ivanescu, L., Duck, T. J., Perro, C., Herber, A., ... and Schrems, O. (2015). Synchronous polar winter starphotometry and lidar measurements at a High Arctic station. Atmospheric Measurement Techniques, 8(9), 3789-3809.

Barreto, A., Cuevas, E., Damiri, B., Guirado, C., Berkoff, T., Berjón, A. J., Hernndez, Y., Almansa, F., and Gil, M. (2013). A new method for nocturnal aerosol measurements with a lunar photometer prototype, Atmos. Meas. Tech., 6, 585-598, doi:10.5194/amt-6-585-2013.

Barreto, A., Cuevas, E., Granados-Munoz, M. J., Alados-Arboledas, L., Romero, M., Gröbner, J., Kouremeti, N., Almansa, A. F., Stone, T., Sorokin, M., Holben, B., Canini, M., and Yela, M. (2015). The new sun-sky-lunar Cimel CE318-T multiband photometer a comprehensive performance evaluation, Atmos. Meas. Tech. Discuss., 8, 11077-11138, doi:10.5194/amtd-8-11077-2015.

Benedetti, A., Morcrette, J.-J., Boucher, O., Dethof, A., Engelen, R. J., Fisher, M., Flentje, H., Huneeus, N., Jones, L., Kaiser, J. W., Kinne, S., Mangold, A., Razinger, M., Simmons, A. J., and Suttie, M. (2009). Aerosol analysis and forecast in the European Centre for Medium-Range Weather Forecasts Integrated Forecast System: 2. Data assimilation, J. Geophys. Res., 114, D13205, doi:10.1029/2008JD011115.

Berkoff, T. A., Sorokin, M., Stone, T., Eck, T. F., Raymond Hoff, R., Welton, E., and Holben, B. (2011). Nocturnal Aerosol Optical Depth Measurements with a Small-Aperture Automated Photometer Using the Moon as a Light Source, J. Atmos. Ocean. Technol., 28, 1297-1306.

Campbell, J. R., Tackett, J. L., Reid, J. S., Zhang, J., Curtis, C. A., Hyer, E. J., Sessions, W. R., Westphal, D. L., Prospero, J. M., Welton, E. J., Omar, A. H., Vaughan, M. A., and Winker, D. M. (2012). Evaluating nighttime CALIOP 0.532 μm aerosol optical depth and extinction coefficient retrievals, Atmos. Meas. Tech., 5, 2143-2160, doi:10.5194/amt-5-2143-2012.

Charlson, R. J. (1969). Atmospheric visibility related to aerosol mass concentration: review. Environmental Science & Technology, 3(10), 913-918.

Chin, M., Diehl, T., Ginoux, P., and Malm, W. (2007). Intercontinental transport of pollution and dust aerosols: implications for regional air quality. Atmospheric Chemistry and Physics, 7(21), 5501-5517.

Diner, D. J., Beckert, J. C., Reilly, T. H., Bruegge, C. J., Conel, J. E., Kahn, R., ... and Verstraete, M. M. (1998). Multi-angle Imaging SpectroRadiometer (MISR) instrument description and experiment overview. Geoscience and Remote Sensing, IEEE Transactions on, 36(4), 1072-1087.

Eck, T. F., Holben, B. N., Reid, J. S., O'Neill, N. T., Schafer, J. S., Dubovik, O., Smirnov, A., Yamasoe, M. A., and Artaxo., P. (2003). High aerosol optical depth biomass burning events: A comparison of optical properties for different source regions. Geophysical Research Letters 30, no. 20.

Elvidge, C. D., Baugh, K. E., Dietz, J. B., Bland, T., Sutton, P. C., and Kroehl, H. W. (1999). Radiance calibration of DMSP-OLS low-light imaging data of human settlements. Remote Sensing of Environment, 68(1), 77-88.

Hair, J. W., Hostetler, C. A., Cook, A. L., Harper, D. B., Ferrare, R. A., Mack, T. L., Welch, W., Izquierdo, L. R., and Hovis, F. E. (2008). Airborne High Spectral Resolution Lidar for profiling aerosol optical properties, Appl. Opt.,47, 67346752, doi:10.1364/AO.47.006734.

Han, H.-J., and Sohn, B. J. (2013). Retrieving Asian dust AOT and height from hyperspectral sounder measurements: An artificial neural network approach, J. Geophys. Res. Atmos., 118, 837845, doi:10.1002/jgrd.50170.

Hansell, R. A., Ou, S. C., Liou, K. N., Roskovensky, J. K., Tsay, S. C., Hsu, C., and Ji, Q. (2007). Simultaneous detection/separation of mineral dust and cirrus clouds using MODIS thermal infrared window data, Geophys. Res. Lett., 34, L11808, doi:10.1029/2007GL029388.

Hao, X., and Qu, J. J. (2007). Saharan dust storm detection using moderate resolution imaging spectroradiometer thermal infrared bands. Journal of Applied Remote Sensing, 1(1), 013510-013510.

Hegg, D. A., Livingston, J., Hobbs, P. V., Novakov, T., and Russell, P. (1997). Chemical apportionment of aerosol column optical depth off the midAtlantic coast of the United States. Journal of Geophysical Research: Atmospheres (19842012), 102(D21), 25293-25303.

Herber, A., Thomason, L. W., Gernandt, H., Leiterer, U., Nagel, D., Schulz, K. H., ... and Notholt, J. (2002). Continuous day and night aerosol optical depth observations in the Arctic between 1991 and 1999. Journal of Geophysical Research: Atmospheres (19842012), 107(D10), AAC-6.

Holben, B. N., Eck, T. F., Slutsker, I., Smirnov, A., Sinyuk, A., Schafer, J., Giles, D., and Dubovik, O. (2006). AERONET's version 2.0 quality assurance criteria. In Asia-Pacific Remote Sensing Symposium (pp. 64080Q-64080Q). International Society for Optics and Photonics.

Holben, B. N., Eck, T. F., Slutsker, I., Tanré, D., Buis, J. P., Setzer, A., Vermote, E., Reagan, J. A., Kaufman, Y. J., Nakajima, T., Lavenu, F., Jankowiak, I., and Smirnov, A. (1998). AERONET - A Federated Instrument Network and Data Archive for Aerosol Characterization, Remote Sens. Environ., 66, 1-16.

Hsu, N. C., Tsay, S. C., King, M. D., and Herman, J. R. (2004). Aerosol properties over bright-reflecting source regions. Geoscience and Remote Sensing, IEEE Transactions on, 42(3), 557-569.

Husar, R. B., Prospero, J. M., and Stowe, L. L. (1997). Characterization of tropospheric aerosols over the oceans with the NOAA advanced very high resolution radiometer optical thickness operational product. Journal of Geophysical Research: Atmospheres (19842012), 102(D14), 16889-16909.

Jackson, J. M., Liu, H., Laszlo, I., Kondragunta, S., Remer, L. A., Huang, J., and Huang, H. C. (2013). Suomi-NPP VIIRS aerosol algorithms and data products. Journal of Geophysical Research: Atmospheres, 118(22), 12-673.

Johnson, R. S., Zhang, J., Hyer, E. J., Miller, S. D., and Reid, J. S. (2013). Preliminary investigations toward nighttime aerosol optical depth retrievals from the VIIRS Day/Night Band, Atmos. Meas. Tech., 6, 1245-1255, doi:10.5194/amt-6-1245-2013.

Joint Polar Satellite System (JPSS) VIIRS Cloud Cover/Layers Algorithm Theoretical Basis Document (ATBD). (2011).
[http://npp.gsfc.nasa.gov/sciencedocs/2015-06/474-00044_Rev-Baseline.pdf]

Kaufman, Y. J., Tanré, D., and Boucher, O. (2002). A satellite view of aerosols in the climate system. Nature, 419(6903), 215-223.

Kaufman, Y. J., Tanré, D., Remer, L. A., Vermote, E. F., Chu, A., and Holben, B. N. (1997). Operational remote sensing of tropospheric aerosol over land from EOS moderate resolution imaging spectroradiometer. Journal of Geophysical Research: Atmospheres (19842012), 102(D14), 17051-17067.

Lanciano, O., and Fiocco, G. (2007). Nighttime measurements of atmospheric optical thickness by star photometry with a digital camera. Applied optics, 46(22), 5176-5182.

Lee, T. E., Miller, S. D., Turk, F. J., Schueler, C., Julian, R., Deyo, S., ... and Wang, S. (2006). The NPOESS VIIRS day/night visible sensor. Bulletin of the American Meteorological Society, 87(2), 191-199.

Lee, S.-S., and Sohn, B. J. (2012). Nighttime AOT retrieval for Asian Dusts from MODIS IR Measurements: An Artificial Neural Network Approach, J. Meteorl. Soc. Jpn., 90, 163-177, DOI:10.2151/jmsj.2012-201.

Legrand, M., Bertrand, J. J., Desbois, M., Menenger, L., and Fouquart, Y. (1989). The potential of infrared satellite data for the retrieval of Saharan-dust optical depth over Africa. Journal of Applied Meteorology, 28(4), 309-319.

Levy, R. C., Mattoo, S., Munchak, L. A., Remer, L. A., Sayer, A. M., and Hsu, N. C. (2013). The Collection 6 MODIS aerosol products over land and ocean. Atmos. Meas. Tech. Discuss, 6, 159-259.

Liou, K. N. (2002). An introduction to atmospheric radiation (Vol. 84). Academic press.

Liu, Y., Liu, R., and Cheng, X. (2013). Dust detection over desert surfaces with thermal infrared bands using dynamic reference brightness temperature differences. Journal of Geophysical Research: Atmospheres, 118(15), 8566-8584.

Ma, X., Bartlett, K., Harmon, K., and Yu, F. (2013). Comparison of AOD between CALIPSO and MODIS: significant differences over major dust and biomass burning regions. Atmospheric Measurement Techniques, 6(9), 2391-2401.

Miller, S. D. (2003). A consolidated technique for enhancing desert dust storms with MODIS, Geophys. Res. Let., 30, 2071, doi:10.1029/2003GL018279.

Omar, A. H., Winker, D. M., Tackett, J. L., Giles, D. M., Kar, J., Liu, Z., Vaughan, M. A., Powell, K. A., and Trepte, C.R. (2013). CALIOP and AERONET aerosol optical depth comparisons: One size fits none, J. Geophys. Res. Atmos., 118, 47484766, doi:10.1002/jgrd.50330.

Pérez-Ramírez, D., Lyamani, H., Olmo, F. J., and Alados-Arboledas, L. (2011). Improvements in star photometry for aerosol characterizations. Journal of Aerosol Science, 42(10), 737-745.

Pérez-Ramírez, D., Lyamani, H., Olmo, F. J., Whiteman, D. N., and Alados-Arboledas, L. (2012). Columnar aerosol properties from sun-and-star photometry: statistical comparisons and day-to-night dynamic. Atmospheric Chemistry and Physics, 12(20), 9719-9738.

Pope III, C. A., and Dockery, D. W. (2006). Health effects of fine particulate air pollution: lines that connect. Journal of the air & waste management association, 56(6), 709-742.

Purkis, S. J., and Klemas, V. V. (2011). Remote sensing and global environmental change. John Wiley & Sons.

Reid, J. S., Hyer, E. J., Prins, E. M., Westphal, D. L., Zhang, J., Wang, J., ... and Hoffman, J. P. (2009). Global monitoring and forecasting of biomass-burning smoke: Description of and lessons from the Fire Locating and Modeling of Burning Emissions (FLAMBE) program. Selected Topics in Applied Earth Observations and Remote Sensing, IEEE Journal of, 2(3), 144-162.

Remer, L. A., Kaufman, Y. J., Tanré, D., Mattoo, S., Chu, D. A., Martins, J. V., ... and Holben, B. N. (2005). The MODIS aerosol algorithm, products, and validation. Journal of the atmospheric sciences, 62(4), 947-973.

Rosenfeld, D., Lohmann, U., Raga, G. B., O'Dowd, C. D., Kulmala, M., Fuzzi, S., ... and Andreae, M. O. (2008). Flood or drought: how do aerosols affect precipitation?. science, 321(5894), 1309-1313.

Schutgens, N. A. J., Miyoshi, T., Takemura, T., and Nakajima, T. (2010). Applying an ensemble Kalman filter to the assimilation of AERONET observations in a global aerosol transport model, Atmos. Chem. Phys., 10, 2561-2576.

Schwartz, S. E. (1996). The whitehouse effectShortwave radiative forcing of climate by anthropogenic aerosols: An overview. Journal of Aerosol Science, 27(3), 359-382.

Smirnov, A., Holben, B. N., Slutsker, I., Giles, D. M., McClain, C. R., Eck, T. F., Sakerin, S. M., ... and Jourdin, F. (2009). Maritime aerosol network as a component of aerosol robotic network. Journal of Geophysical Research: Atmospheres (19842012) 114, no. D6.

Wald, A. E., Kaufman, Y. J., Tanré, D., and Gao, B. C. (1998). Daytime and nighttime detection of mineral dust over desert using infrared spectral contrast. Journal of Geophysical Research: Atmospheres (19842012), 103(D24), 32307-32313.

Welton, E. J., Campbell, J. R., Berkoff, T. A., Valencia, S., Spinhirne, J. D., Holben, B., ... and Schmid, B. (2006). The NASA Micro-Pulse Lidar Network (MPLNET): an overview and recent results. Opt. Pur. y Apl, 39, 67-74.

Winker, D. M., Vaughan, M. A., Omar, A., Hu, Y., Powell, K. A., Liu, Z., ... and Young, S. A. (2009). Overview of the CALIPSO mission and CALIOP data processing algorithms. Journal of Atmospheric and Oceanic Technology, 26(11), 2310-2323.

Wong, M. S., Xiao, F., Nichol, J., Fung, J., Kim, J., Campbell, J. R., and Chan, P. W. (2015). A multi-scale hybrid neural network retrieval model for dust storm detection, a study in Asia. Atmospheric Research, 158, 89-106.

Xiao, F., Wong, M. S., Lee, K. H., Campbell, J. R., and Shea, Y. K. (2015). Retrieval of dust storm aerosols using an integrated Neural Network model. Computers & Geosciences.

Zhang, J., Campbell, J. R., Hyer, E. J., Reid, J. S., Westphal, D. L., and Johnson, R. S. (2014). Evaluating the impact of multisensor data assimilation on a global aerosol particle transport model. Journal of Geophysical Research: Atmospheres, 119(8), 4674-4689.

Zhang, J., Reid, J. S., Westphal, D. L., Baker, N. L., and Hyer, E. J. (2008a). A system for operational aerosol optical depth data assimilation over global oceans, J. Geophys. Res., 113, No. D10, D10208, doi: 10.1029/2007JD009065.

Zhang, J., Reid, J. S., Miller, S. D., and Turk, F. J. (2008b). Strategy for studying nocturnal aerosol optical depth using artificial lights, Int. J. Remote Sens., Vol. 29, No. 16, 4599-4613, doi: 10.1080/01431160802020528.